







# Testing and Combining Transient Spectral Classification Tools on 4MOST-like Blended Spectra

A. Milligan<sup>1</sup>   I. Hook<sup>1</sup> , C. Frohmaier<sup>2</sup> , M. Smith<sup>1</sup>, G. Dimitriadis<sup>1</sup> Y.-L. Kim<sup>1</sup> , K. Maguire<sup>3</sup>,  
A. Moller<sup>4</sup>, M. Nicholl<sup>5</sup>, S. J. Smartt<sup>5,6</sup>, J. Storm<sup>7</sup>, M. Sullivan<sup>2</sup>, E. Tempel<sup>8</sup>, P. Wiseman<sup>2</sup> , L. P. Cassarà<sup>9</sup>,  
R. Demarco<sup>10</sup>, A. Fritz<sup>11</sup>, J. Jiang<sup>12, 13</sup>

<sup>1</sup>Department of Physics, Lancaster University, Lancs LA1 4YB, UK

<sup>2</sup>School of Physics and Astronomy, University of Southampton, Southampton, SO17 1BJ, UK

<sup>3</sup>School of Physics, Trinity College Dublin, The University of Dublin, Dublin 2, Ireland

<sup>4</sup>Centre for Astrophysics & Supercomputing, Swinburne University of Technology, Victoria 3122, Australia

<sup>5</sup>Astrophysics Research Centre, School of Mathematics and Physics, Queens University Belfast, Belfast BT7 1NN, UK

<sup>6</sup>Astrophysics Sub-department, Department of Physics, University of Oxford, Keble Road, Oxford OX1 3RH, UK

<sup>7</sup>Leibniz-Institut für Astrophysik Potsdam (AIP) An der Sternwarte 16, 14482 Potsdam

<sup>8</sup>Tartu Observatory, University of Tartu, Observatooriumi 1, Tõravere 61602, Estonia

<sup>9</sup>INAF-IASF Milano, via Alfonso Corti 12, 20133 Milano (Italy)

<sup>10</sup>Institute of Astrophysics, Facultad de Ciencias Exactas, Universidad Andrés Bello, Sede Concepción, Talcahuano, Chile

<sup>11</sup>Kuffner Observatory, Johann-Staud-Strasse 10, 1160 Vienna, Austria

<sup>12</sup>Institute of Astronomy, University of Cambridge, Madingley Road, Cambridge CB3 0HA, UK

<sup>13</sup>Department of Physics, University of Warwick, Gibbet Hill Road, Coventry CV4 7AL, UK

Accepted XXX. Received YYY; in original form ZZZ

## ABSTRACT

With the 4-meter Multi-Object Spectroscopic Telescope (4MOST) expected to provide an influx of transient spectra when it begins observations in early 2026 we consider the potential for real-time classification of these spectra. We investigate three extant spectroscopic transient classifiers: the Deep Automated Supernova and Host classifier (DASH), Next Generation SuperFit (NGSF) and SuperNova IDentification (SNID), with a focus on comparing the efficiency and purity of the transient samples they produce. We discuss our method for simulating realistic, 4MOST-like, host-galaxy contaminated spectra and determining quality cuts for each classifier used to ensure pure SN Ia samples while maintaining efficient classification in other transient classes. We investigate the classifiers individually and in combinations. We find that a combination of DASH and NGSF can produce a SN Ia sample with a purity of 99.9% while successfully classifying 70% of SNe Ia. However, it struggles to classify non-SN Ia transients. We investigate photometric cuts to transient magnitude and transient flux fraction, finding that both can be used to improve transient classification efficiencies by 7–25% depending on the transient subclass. Finally, we present an example classification plan for live classification and the predicted purities and efficiencies across five transient classes: Ia, Ibc, II, superluminous and non-supernova transients.

**Key words:** transients: supernovae; techniques: spectroscopic; software: simulations; software: machine learning; instrumentation: spectrographs.

## 1 INTRODUCTION

Since the discovery of the accelerating expansion of the universe a quarter of a century ago (Perlmutter et al., 1999; Riess et al., 1998), significant efforts have been made to investigate the enigmatic properties of dark energy. Many probes into the nature of dark energy exist, including weak lensing and Cosmic Microwave Background measurements (Planck Collaboration et al., 2014; Wittman et al., 2000). However, one of the most successful at providing strong constraints on cosmological models in the late-time universe is type Ia

supernova (SN) cosmology. Understood to be the detonation of white dwarfs around the Chandrasekhar mass limit, SNe Ia detonate at predictable luminosities and as such act as standardisable candles that let us measure the distance to objects over large swathes of cosmic time.

The original discovery of accelerating expansion was performed with a sample of only 42 high-redshift SNe Ia (Perlmutter et al., 1999). Since then, we have seen an order of magnitude increase in the number of spectroscopically confirmed SNe Ia. The recent first data release from the Zwicky Transient Facility (ZTF) contains 761 spectroscopically confirmed SNe Ia (Dhawan et al., 2022) and

\* E-mail: a.milligan@lancaster.ac.uk

the Pantheon+ sample contains 1,550 unique, spectroscopically confirmed SNe Ia (Scolnic et al., 2022).

Most optical transients are discovered in photometric surveys. As the number of transients has increased, it has become unfeasible to allocate time for spectroscopic follow-up on each transient individually. Recent photometric classifiers can perform high accuracy classification on transients beyond just classifying them as SN Ia or non-SN Ia. Additionally, it has been shown that they are capable of classifying transients based on incomplete light curves (Möller & de Boissière, 2020). Recent photometric analyses have indicated that SN Ia samples obtained with photometric classifications produce contamination levels that either still allow for robust estimations of cosmological parameters or are even negligible compared to other sources of uncertainty (Jones et al., 2018, 2019; Vincenzi et al., 2024).

While photometric classification is possible, it has several distinct disadvantages. The definitions of SN subclasses are based primarily by spectral features, so spectroscopic classification removes ambiguity. Further, photometric classification often still requires some spectroscopic information. In Vincenzi et al. (2024) 1,635 photometrically classified SNe Ia are used for cosmology, the largest single-survey SN Ia sample, but classification was performed with spectroscopic redshifts and a smaller sample of spectroscopically classified SNe Ia were used to anchor the cosmological fits (see also DES Collaboration et al., 2024b). Additionally, to match the high purities of spectroscopically classified transient sample, photometric classification is usually performed in a binary scheme (SN Ia vs non-SN Ia) or with very broad transient classes (Fraga et al., 2024).

We will, therefore, test the performance of spectroscopic classifiers. The earliest samples of transients were separated into two classes: SNe I and SNe II, based on the presence or absence of Hydrogen features in their spectra (Popper, 1937; Minkowski, 1979). In the years since, these classes have been further subdivided and many new subclasses and exotic variants have been discovered and suggested, alongside non-supernova transients like Tidal Disruption Events (TDEs) and Fast Blue Optical Transients (FBOTs) (Gezari, 2021; Drout et al., 2014). Visual classification is made difficult by the overlap of various transient subclasses in parameter space and ambiguity in subclass definitions. This, alongside the increasing number of transients being observed spectroscopically, means that it is increasingly required to automate the process of spectroscopic classification. We seek to investigate the potential to do this with regards to the upcoming 4MOST instrument.

The 4-metre Multi-Object Spectrograph Telescope (de Jong et al., 2019, 4MOST) is a high-multiplex, fibre-fed spectrographic survey facility in the final stages of assembly before commissioning. It is expected that it will begin taking data in early 2026. There are many varied surveys within the 4MOST consortium, but the survey concerned with transients is the Time Domain Extragalactic Survey (TiDES) (Swann et al., 2019).

With the upcoming Legacy Survey of Space and Time (LSST) being performed from the Vera C. Rubin Observatory, there will be unprecedented numbers of transients discovered photometrically (Ivezić et al., 2019). It is expected that any given pointing of 4MOST will contain a number of live photometric transients and the host galaxies of faded transients, which can then be followed-up with TiDES's allotted fibres. Over a period of 5 years, TiDES expects to observe 35,000 live transients and perform follow-up on some 50,000 host galaxies (these numbers are dependent on the survey schedules of LSST and 4MOST, both of which are still under development). This approach has already seen success in the Australian Dark Energy Survey (OzDES) performed using the AAOmega spectrograph on the

Anglo-Australian Telescope (Lidman et al., 2020; Saunders et al., 2004).

Two of TiDES science goals are to provide live classification of transients accessible to the general scientific community and the classification of a large, pure, cosmological SN Ia sample. As we approach data being taken, uncertainty remains as to how the TiDES transient spectra will be classified and which existing spectroscopic classifiers, if any, are best suited to these two TiDES science goals. Our hope is to provide clarity via the simulation of transient spectra that are as close to what will be observed as possible, including the fact that transient flux observed by a 4MOST fibre will be blended with the flux of its host galaxy. These realistic, blended, simulated 4MOST spectra will allow us to compare the output of various spectroscopic classifiers to known true classifications (See also Kim et al., 2024, which makes use of real spectra in its analysis). Furthermore, we can assess the dependence of classification performance on parameters such as the brightness of the SN and the fraction of host light contaminating the spectrum, and ultimately use this information to outline a plan for the classification of large numbers of TiDES spectra.

There are two main types of automated, spectroscopic classifiers. First, there are template matching programs (for example, Duan et al., 2009; Blondin & Tonry, 2011; Goldwasser et al., 2022). These compare an input spectrum to a bank of transients of known classification. The bank spectra can be redshifted iteratively and the best-fitting spectrum and redshift provide a classification and an estimate of spectroscopic redshift.

More recent years have seen the rise of the second type: machine-learning methods (for example, Muthukrishna et al., 2019; Vogl et al., 2020). In this case, a classifier is provided a training set of templates of known classification and redshift. The classifier "learns" the features present in various transient classifications and assigns them weights. The presence or not of these learned features is then used to determine the probability of an input spectrum belonging to a given classification.

In this paper we investigate two template-matching classifiers and one machine-learning classifier. More information on the spectroscopic transient classifiers we investigate can be found in Sections 4.1, 4.2 and 4.3.

Hence, this paper is organized as follows. First, in Section 2, we describe the simulations from which we draw our transient and host properties. Also in this Section we will discuss some transient templates used in simulating our blended spectra. In Section 3, we will discuss the construction of blended host-transient spectra and the subsequent simulation of 4MOST observations using an Exposure Time Calculator (ETC). Then, in Section 4, we investigate the capabilities of three individual spectroscopic transient classifiers. We go over their function and how they were tested. We investigate the combination of classifiers in Section 5. The direct comparison is first performed in Section 5.1, and then potential photometric cuts for improving classification in Section 5.3. Finally, in Section 5.4 we present a potential classification pipeline for live classification and SN Ia cosmology. Our conclusions are presented in Section 6.

## 2 DATA

### 2.1 Survey Simulations

Our objective is to test spectroscopic transient classifiers such that we understand under what conditions they will succeed or fail when used on 4MOST-like spectra. As such we must simulate a set of

spectra that are a good approximation to the real ones observed by the instrument. The specific procedure for the creation of individual spectra is covered more in Section 3, but we first discuss how we obtain a set of realistic properties for transients and their hosts. These properties can then be used to generate each spectrum, which in turn can be used to test each of the pre-existing transient classifiers. The results of these classifications can then be compared to the input spectrum's 'true' properties as a means to quantify the success of a given classifier.

There are two pre-existing simulations from which transient and host properties are retrieved. The first is a TiDES-specific simulation of a population of transients and hosts performed in the SUPernova ANALYSIS package (Kessler et al., 2009, SNANA). SNANA uses known intrinsic properties of various transient classes in combination with the survey strategy of the LSST survey to generate an LSST-specific transient population (Frohmaier et al., in prep.). These simulations produce a population of transient and host objects. From them we obtain the intrinsic physical properties of host–transient systems. We obtain system redshift, host–transient separation, host  $r$ -band magnitude and transient template information. The process of creating simulated spectra is discussed in more detail in Section 3.

The second simulation is a simulation of the 4MOST survey operation of the full 5 years of observations of the southern sky. Observation targets are taken from the simulated survey input catalogs and their exposure times are computed using the 4MOST Exposure Time Calculator (ETC). The simulation is carried out with the 4MOST facility simulator (4FS) and makes use of the simulation code SELFIE. More detail about the SELFIE algorithm can be found in Tempel et al. (2020a,b).

This simulation provides further observational properties for each transient. Most importantly, from it we receive a list of all of the transients that were observed. Generally, any transient that is both located within 4MOST's field of view during a visit, and is estimated to require less exposure time than is available during the full visit to meet the TiDES spectral success criterion (average  $SNR > 3$  in 15 Å bins in the wavelength range of 4500–8000 Å) will be observed. However, some are not observed due to the limited number of fibres and the demands of other subsurveys.

As the simulations have become more sophisticated, different versions of the input catalogue have been created. Each has had many different simulations of survey operations performed on it. We find that while the individual objects observed may change dramatically between simulations, the bulk properties of the observed transients are consistent. As such the specific simulation used has little effect on our final results.

The 4MOST observing schedule is currently expected to visit each sky position a small number of times during the 5-year survey. Each visit to a given position will consist of several exposures (most often 2 or 3) of approximately 20 minutes. The reported exposure time available for a given visit is the exposure time we will assume for any transients contained in that visit.

The majority of repeat visits to the same transient objects in the general extra-galactic sky fields occur with sufficient interim time that the transient's spectrum will have evolved significantly. This is useful for tracking spectral evolution, but not for stacking spectra to improve the SNR.

The  $r$ -band magnitude, redshift and SN flux fraction distributions of the observed transients and their hosts from the SNANA population simulation are shown in Fig. 1. The total number of objects in the sample is on the order of  $10^5$ . We see that the sample is heavily biased to  $z < 0.6$  and in fact the more distant objects are

all Superluminous Supernovae (SLSNe). We also see that, before any correction for fibre sizes, when observing extended objects (see Section 3.3) there is a tendency for host galaxies to have brighter magnitudes than transients.

## 2.2 Simulated Spectra

In addition to realistic physical and observational properties for use in creating simulated 4MOST-like spectra, we require a set of spectral templates of both transients and hosts. The transient templates are drawn from those used in the SNANA population simulations. The included SN classes are Ia, Ib, Ic, II, IIn, IIB and SLSNe. All SNe Ia input templates are of the Ia-norm subclass, generated using the SALT2 model. Additionally there are tidal disruption events (TDEs), and calcium-rich transient (CaRT) objects. These templates are spectral energy distributions intended to simulate realistic photometry. As such, some of the spectra, especially SLSNe and non-SN transient, are highly smoothed and lacking in spectroscopic features. The full list of template sources is provided in Table 1.

The galaxy templates from Kinney et al. (1996) are assigned as hosts. The subclasses of galaxy available are elliptical, S0, Sa, Sb and Sc and a set of starburst templates with a variety of E(B-V) values (see Kinney et al. (1996) for additional information).

We use the  $r$ -band host magnitudes from the simulation. Assignments of host galaxies are based on the work of Hakobyan et al. (2012), in particular the relative transient rates presented in their Table 5. For elliptical and S0-Sc templates we assign hosts randomly to match the proportions presented in Hakobyan et al. (2012). For Sd and Irregular galaxies for which we have no templates, we assign a random choice between Sb and Sc host spectra (the two most common host morphologies). In cases where Hakobyan et al. (2012) lists the host as Morphology A/Morphology B, we choose randomly between A and B. We always assign SLSNe inputs an Sc-type host spectrum since research suggests that SLSNe are found in faint, blue, star-forming galaxies, often with extreme emission lines (Leloudas et al., 2015; Neill et al., 2011). No host distributions are reported for TDEs or CaRTs. Since these occupy such a small percentage of our transients, we assign them a host type at random.

In this paper we make use of two sets of transient objects. Each is derived from the sample of objects from the population simulation that were observed in the survey simulation as shown in Fig. 1.

The first sample consists of 100 transients. This is made up of 60 SNe Ia, which are expected to be the majority of real transients observed, and 5 of every other transient observed in survey simulation (II, IIn, IIB, Ib, Ic, SLSNe, TDE and CaRT). This sample is used to define the quality cuts applied to the classifications from each classifier and as such will subsequently be referred to as the quality control sample.

The second sample contains spectra for all observed transients in the survey simulation. This sample is used for the final classifier comparison results in Section 5 and so it will be referred to as the comparison sample for the rest of the paper. A breakdown of the transient classes contained in the comparison sample are provided in Table 1.

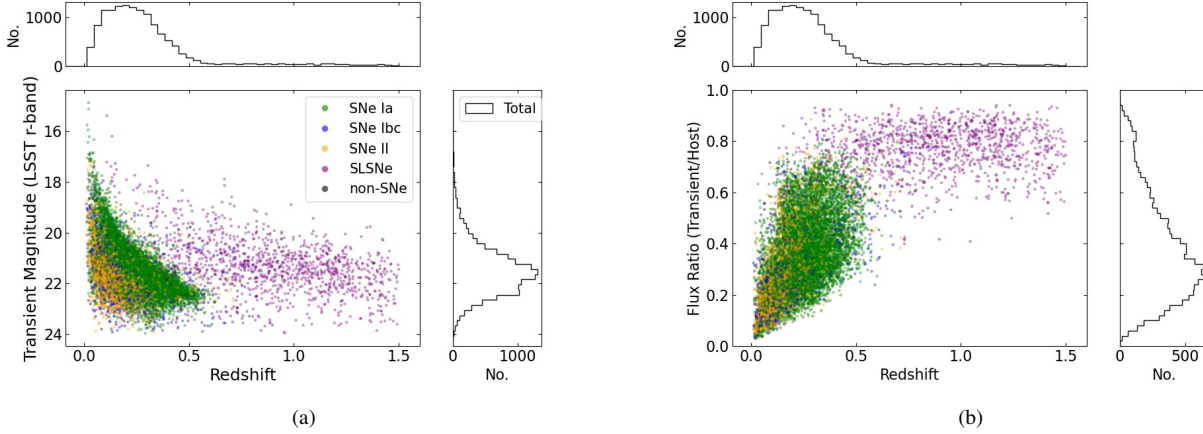


**Figure 1.** a) Host galaxy redshift and corresponding transient magnitudes for observed objects in the SELFIE survey simulation. The values are obtained directly from the SNANA population simulation and can be considered the truth values for a given object. The y-axis on the attached histograms displays the total number of objects per bin. b) As in (a) but with the fraction of fibre flux from the transient on the y-axis. Magnitudes are uncorrected for fibre losses or seeing.

**Table 1.** The relative percentages of each transient class present in the comparison sample alongside the sources for the transient templates. SN Ia-91bg templates are provided by Kessler et al. (2019), with all other SN Ia templates provided by Guy et al. (2007) and Hounsell et al. (2018). The comparison sample will be used to compare the results from the transient classifiers discussed in Section 5.

Percentage	Class	Source
61.3%	SNe Ia	Guy et al. (2007), Hounsell et al. (2018) Kessler et al. (2019)
2.0%	SNe Ib	Vincenzi et al. (2019)
1.5%	SNe Ic	Vincenzi et al. (2019)
13.8%	SNe II	Vincenzi et al. (2019)
6.7%	SNe IIn	Vincenzi et al. (2019)
4.1%	SNe Iib	Vincenzi et al. (2019)
9.6%	SLSNe	Kessler et al. (2019)
0.7%	TDE	Kessler et al. (2019)
0.4%	CaRT	Kessler et al. (2019)

### 3 CREATING BLENDED SPECTRA

#### 3.1 The 4MOST Exposure Time Calculator

The 4MOST ETC python code package<sup>1</sup> allows one to simulate an observation by the 4MOST instrument. For every simulated observation we must assign a brightness within a specific filter or over a wavelength range. A variety of pre-existing instrument filters are provided. Throughout this paper magnitudes are calculated using the LSST *r*-band filter and are reported in the AB magnitude system (Oke & Gunn, 1983).

The code produces a ‘raw’ or Level 0 (L0) output and a Level 1 (L1) output. Both are in the form of extracted 1D spectra (flux and wavelength for each pixel along the spectrum). The raw output features 4MOST’s three spectrograph arms not yet combined and the object flux reported in ADUs. The L1 output is what we use. L1 spectra are generated by being passed through a simulation of the Quality Control 1 (QC1) pipeline and resemble the data products that will be produced by the real instrument. In L1 output, the ADUs of the

raw output are converted to a flux observed at the telescope entrance using corrections for the wavelength dependence of the instrument’s sensitivity.

The simulation process is shown in Fig. 2. There are still telluric absorption bands present in the L1 output which are added as part of the ETC model. There are five main features with wavelength ranges of 6250 – 6350, 6860 – 6940, 7150 – 7350, 7550 – 7700 and 8100 – 8400 Å. These extra features could be misinterpreted by classifiers as being generated by the transient and lead to misclassifications. We account for this by creating a transmission spectrum for each observation. We do this on the assumption that real data will have these features corrected for using 4MOST observations of featureless calibration stars.

We consider the host and transient separately before adding them linearly to form the final spectrum that is input into the ETC for a simulated observation. The magnitudes of both objects are known from the population simulation, but to account for seeing conditions and a finite fibre size on extended galaxies we must adjust these magnitudes. The processes for doing so for SNe and galaxies are shown in detail in Sections 3.2 and 3.3 respectively.

#### 3.2 Transient Fibre Flux

We assume the transient can be approximated as a point source and that the 4MOST fibre will be placed centrally on the transient. We simulate the fraction of transient flux through a 4MOST fibre using a grid of pixels with a central pixel containing the full transient flux. A Gaussian convolution is then applied to the pixel grid. The standard deviation,  $\sigma$ , of the Gaussian convolution is determined from the Full-Width Half-Maximum (FWHM) of the seeing conditions using the expression  $\text{FWHM} = 2\sqrt{2 \ln 2} \sigma$ .

The SELFIE simulations do not record seeing conditions for each observation. For our purposes the seeing conditions are taken to always have a value of 0.8 arcseconds, this is similar to the average seeing conditions found at the Paranal Observatory where 4MOST will be located<sup>2</sup>.

<sup>1</sup> We use V2.3.1 of the python-based ETC: See [qmostetc link to documentation](#)

<sup>2</sup> From Paranal Observatory website, <https://www.eso.org/gen-fac/pubs/astclim/paranal/seeing/>, accessed 23-January-2024



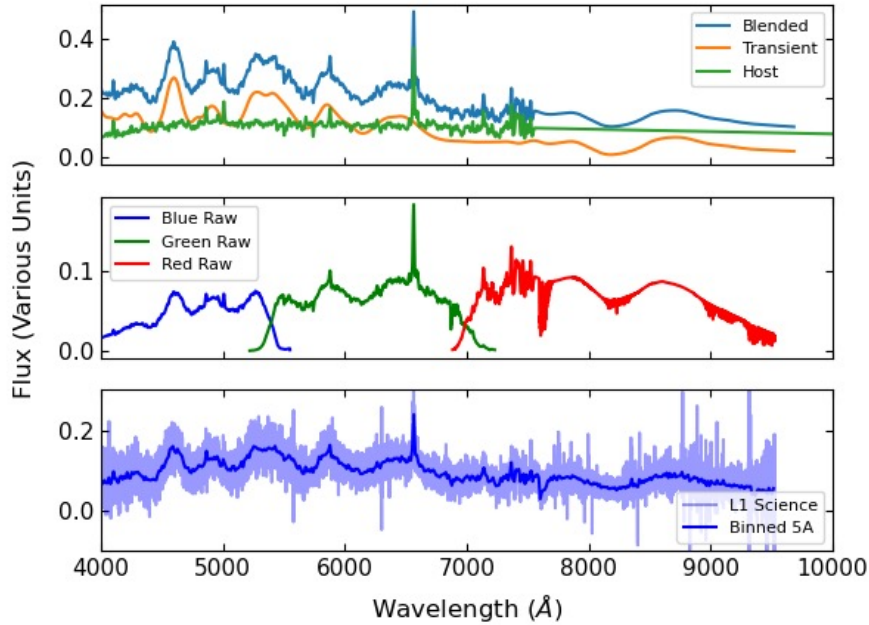


**Figure 2.** The stages of simulating an observation with the 4MOST ETC code. In this example, a 21st magnitude SN Ia and a 21st magnitude Sc-type host spectra are added linearly. Top panel: template SN, host and combined spectra. All spectra are at zero redshift. The flux is measured in units of  $\text{erg cm}^{-2} \text{s}^{-1} \text{\AA}^{-1} \times 10^{-16}$ . This is the input to the ETC. Middle panel : L0 output of the ETC, showing the extracted spectra from the three spectrograph arms. Flux is presented in units of  $e^- \times 10^3$ . Lower panel: L1 output of the ETC in which the spectra from the three arms have been joined. The result is flux-calibrated and includes a realisation of the noise. This (unbinned) L1 spectrum is what we perform classification on. The units of flux are the same as in the top panel.

Once the Gaussian convolution has been applied, a fibre with a 4MOST fibre diameter of 1.45 arcseconds is imposed onto the pixel grid, centred on the SN location. The flux is then summed from the pixels with centres contained within the fibre radius. We find that using a finer pixel grid produces a more accurate value for fibre flux by reducing uncertainty around the fibre edge. This is particularly important in Section 3.3 where the scale of hosts being modelled varies and a balance must be found between accuracy and computation time.

We are assuming a constant value for the seeing, coupled with a constant fibre size, so we see a constant fraction of transient flux down each fibre. The effect is that each transient appears 0.13 magnitudes fainter through the 4MOST fibre.

### 3.3 Host Fibre Flux

The modelling of fibre flux from the transient’s host galaxy, an extended object, is more complex. This method involves the dimensionless distance parameter ( $d_{DLR}$ ), first used in Sako et al. (2018), in service of assigning hosts to transients and based on similar methods developed in Sullivan et al. (2006). The  $d_{DLR}$  is equal to the ratio of the directional light radius (DLR) of a galaxy and its observed separation from the transient. The DLR is the half-light radius of the galaxy in the direction of the transient. Minimising the  $d_{DLR}$  for galaxies in a crowded field indicates likely hosts for the transient.

The population simulation we draw SNANA-produced physical properties from reports both the  $d_{DLR}$  and the host–transient separation. Since we are only concerned with the host’s flux in the direction of the transient for the purposes of measuring the flux through a

4MOST fibre, we can consider all galaxies in the simulation to have circular half-light radii equal in radius to their DLRs.

We model the intensity of the galaxy to be a Sérsic profile and use a Sérsic index of 0.5 based on values reported in the simulations (Sérsic, 1963). While this may not be completely true to life, it represents the case with the most host flux in a blended spectra and the hardest spectra to classify. Using a larger Sérsic index causes the average host flux in the fibre to decrease leading to less host contamination. The sérsic profile is dependent on the value of the constant  $b_n$  which in turn is defined by the Sérsic index. A number of approximations for the value exist such as  $b_n = 1.9992n - 0.3271$  for  $0.5 \leq n \leq 10$  from Capaccioli (1989) and  $b_n = 2n - \frac{1}{3} + 0.009876n$  from the appendices of Prugniel & Simien (1997). We will use the latter.

The intensity profile, in terms of the Sérsic index,  $n$ , and  $b_n$ , is often expressed as:

$$I(R) = I_e \exp\left\{-b_n \left[\left(\frac{R}{R_e}\right)^{\frac{1}{n}} - 1\right]\right\} \quad (1)$$

where  $R_e$  is the effective or half-light radius that encircles half of the total emission of the profile. The effective intensity,  $I_e$ , is the intensity at the effective radius.

To obtain the ratio of total galaxy flux to the flux transmitted through the fibre, we need to know the value of the total flux and the effective intensity. The total flux is obtained by integrating the intensity profile in equation 1 which leads to the equation:

$$F_T = 2.8941\pi I_e R_e^2 \quad (2)$$

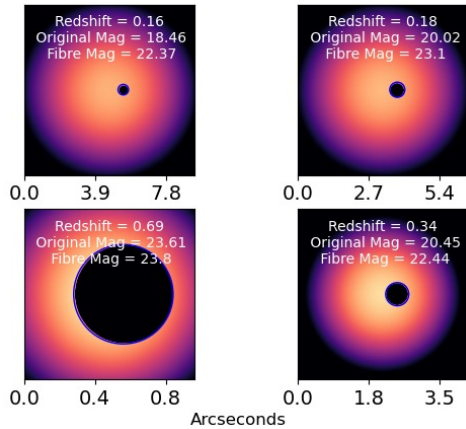


**Figure 3.** The variation in the host flux through 4MOST fibres. Each panel presents the Sérsic profile of an example host galaxy in our sample simulated on a pixel grid. Superimposed as a blue circle is the 4MOST fibre of diameter 1.45", centred on the transient location. The pixels that contribute to the flux seen by the fibre have their flux set to zero in these images, so that the lost flux can be seen. Redshifts, and host magnitude before and after accounting for fibre losses are provided.

This gives us the total flux in terms of the effective intensity and the effective radius which is just the DLR (For a more detailed derivation see [Graham & Driver, 2005](#), and references therein). We can find the actual value of the total flux, and thus a value for the effective intensity, from the zero point magnitude of the AB magnitude system and the total magnitude of the galaxy,  $m_G$ , using the equation:

$$F_T = f_0 \times 10^{(m_G/-2.5)} \quad (3)$$

Here  $f_0$  is the zero point flux of the AB magnitude system. The total host flux,  $F_T$ , that appears in our equations only functions as a scaling factor. We know the true value of  $m_G$  from the population simulation. By taking the ratio of total flux to flux in the 4MOST fibre, the value of the total flux cancels out and so it need not be calculated specifically. Once an arbitrary total flux is chosen we can calculate the effective intensity,  $I_e$ , using equation 2. We can then use equation 1 and equation 2 to calculate the ratio between the total flux, the flux down the fibre and thus the host's magnitude as observed by 4MOST down its fibre.

We simulate a host's intensity profile by creating a pixel grid and use the Sérsic profile to determine the average intensity at each pixel. Since we only care about the host's light profile in the direction of the transient, we model each host as a circle with a half-light radius equal to the DLR.

We then apply a Gaussian convolution to the pixel grid to account for atmospheric seeing. The method is identical to that described in Section 3.2. We centre the fibre on the transient location and calculate the fraction of flux in the fibre. The results of this process are shown in Fig. 3.

We see much more significant flux loss than for the SNe as discussed in Section 3.4. We use a 1,200 x 1,200 pixel grid with each pixel set to 1% of the host-transient separation, where the flux fraction is consistent as pixel size is subject to small variations.

The 4MOST ETC cannot simultaneously account for both extended and point sources in a simulated observation. This is why we account for fibre losses and seeing effects ourselves, prior to passing

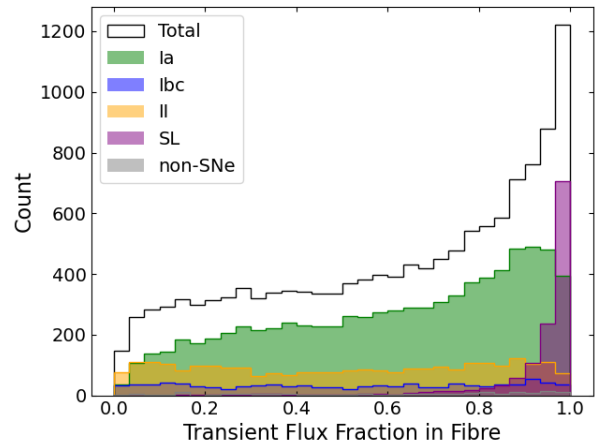


**Figure 4.** The distribution of transient flux fractions in the fibre. As this is in the fibre, this plot follows both transient and host magnitudes being corrected for seeing and fibre effects. The mean value is highlighted with the dashed black line. As this accounts for fibre losses in the host galaxy, we see that over half of all of the spectra have more transient flux than host flux through the 4MOST fibre.

the blended spectrum to the ETC. We provide the blended spectrum as being a flat illumination source with brightness measured in magnitudes per square arcsecond to prevent the ETC from reapplying any observational effects like seeing.

### 3.4 Effect on Galaxy Magnitudes

As stated in Section 3.2, the effect on the transient magnitude is fairly minimal. Most of the flux from the original point source still falls within the fibre that has a diameter of roughly  $2\sigma$  relative to the Gaussian convolution. For hosts, their distance, size and separation from their hosted transient result in significantly more variation in the fraction of the flux that is seen by the fibre (see Fig. 3). This is a critical effect to model. By correcting the host magnitudes for fibre effects we see an average increase in the host magnitude of about 3.1 mag. This leads to significantly improved classification ability for these spectra as the effective host flux in the fibre is significantly reduced.

Usually, classifier performance improves with a greater fraction of transient flux in the fibre (see Section 5.3.2). Performance drops off significantly when the host flux contributes half or more of the total fibre flux. The distribution of transient fibre flux fractions shown in Fig. 4 demonstrates that we now have more than half of our spectra that are transient-flux dominated and within the highly classifiable regime.

## 4 TESTING CLASSIFIERS

With simulated transient spectra realistically blended with host galaxy flux now in hand, we can begin to test our spectroscopic classifiers. We will be testing the Deep Automated Supernova and Host classifier (DASH, [Muthukrishna et al., 2019](#)), Next Generation SuperFit (NGSF, [Howell et al., 2005](#)) and SuperNova IDentification (SNID, [Blondin & Tonry, 2011](#)). These classifiers are introduced in Sections 4.1, 4.2 and 4.3, respectively. We note that we run the classifiers in non-interactive mode to mimic an automated

classification plan for very large numbers of spectra. This is not the way these classifiers were intended to run, and a drop in performance is expected as a result.

Our objective is to compare the performance of each classifier on our simulated spectra. In this section, for each classifier, we will perform a classification on a small subset of the observed transients in the survey simulation (the quality control sample defined in Section 2.2). Each classifier assigns some form of quality metric to the output classifications. In this section we also seek to determine quality cuts for these classification metrics. Then we will compare their performances on the full set of transients (the comparison sample defined in Section 2.2) using our classification metric cuts in Section 5.

The standards by which we will judge the performance of the classifiers are the purity and efficiency of their classifications. Purity and efficiency are, for a target transient class, defined as:

$$\text{Purity} = \frac{\text{TP}}{\text{TP} + \text{FP}} \quad (4)$$

$$\text{Efficiency} = \frac{\text{TP}}{\text{TP} + \text{FN}} \quad (5)$$

Here TP (true positive) are the number of spectra of the target class identified as such. FP (false positive) is the number of non-target class spectra misclassified as such. FN (false negative) is the number of target class spectra misclassified out of the target class. TN (true negative) classifications are spectra correctly identified as not being in the target class.

Outside of binary classifications, for a given transient class, the efficiency is the fraction of that class that are successfully identified as such. The purity is the fraction of output classifications of that class which are correct. Thus the rate of contamination in a transient class is  $1 - \text{purity}$  for that class.

Additionally, in Section 14, we will make use of the classification accuracy of our classifiers. This is particularly useful for comparison to photometric classifiers, which often use this parameter to quantify success. Accuracy is the fraction of classifications across all classes that are correct. In a binary schema it is defined as:

$$\text{Accuracy} = \frac{\text{TP} + \text{TN}}{\text{TP} + \text{TN} + \text{FP} + \text{FN}} \quad (6)$$

We have a focus on producing large and pure SN Ia samples. As such we will focus on the classifier's efficiency and purity in classifying SNe Ia, while also tracking the efficiencies in classifying non-SN Ia transients. We will adopt 95% as an acceptable purity in our SN Ia sample to allow for subsequent cosmological analysis. This is a reasonable contamination compared to others in the literature. For example, Howell et al. (2005) reported an 8% non-SN Ia contamination rate (92% purity) in their final sample of SNe Ia, while Campbell et al. (2013) reported a 3.9% predicted contamination rate (96.1% purity) that has an insignificant effect on their cosmological measurements. In Guy et al. (2010) purity ranges from 100% to 90% are found in various redshift bins up to  $z = 1$  and again, they report that the effect on cosmology is minimal compared to other sources of error.

In this section we will be considering a binary classification. SNe will either be classified as a SN Ia or a non-SN Ia transient. This is far fewer classes than each classifier has the potential to output. We will also be tracking non-SN Ia transients that are misclassified as Ia contaminants. For a SN Ia input to result in a successful classification

we require that a classifier output a cosmologically useful SN Ia subclass and meet any other individual quality limits. Since we have no input SNe Ia spectra that are not cosmologically useful, any peculiar SN Ia output classifications are automatically considered misclassifications. The list of cosmologically useful SN Ia, peculiar SN Ia and non-SN Ia classification bins for each classifier are included in Table 2.

Additionally, we will make use of a classification system that includes six transient classes: SNe Ia, SNe Ibc, SNe II, SLSNe, non-SN transients and 'other' classifications, following the work of Kim et al. (2024). The breakdown of classifier output subclasses that correspond to each of these inputs is also indicated in Table 2. The 'other' class operates as a catch-all, containing Ia-pec subclasses, misclassifications and correct classifications of insufficient quality. For the purposes of calculating efficiencies, classifications that end up in the 'other' class are considered FNs.

Our general method to determine whether a classification is of good quality is as follows. First, we check if the predicted classes of the classification matches the true input template class. If they match then we perform further checks: we check if the first best-fitting class' quality metric is greater than some chosen threshold. If yes, then the classification is considered good. We check the 'reliability' of the classification by checking for agreement between the subclasses of the three best-fitting output subclasses. Reliable results can be subject to less stringent quality cuts. DASH produces a 'reliability' flag as standard. A more detailed outline is provided in Fig. 5.

Some examples of successful and unsuccessful classifications are shown in Appendix B.

## 4.1 DASH

### 4.1.1 Using DASH

DASH is a deep convolutional neural network. We will start by giving an overview of the functionality of DASH. We then discuss our rules for good and 'other' classifications in terms of the *rlap* and probability limits. In section 4.1.2 we report our attempt to assign a value to each of these limits.

DASH is trained on a set of templates and learns spectral features. Input spectra are broken down into individual features, compared to the features in the training set and then assigned a probability to each of its classification bins. The highest probabilities are then summed, assuming they all agree on the best-fitting transient class, to create a single probability for that best class called the Softmax percentage. This is not necessarily a judgement on the quality of the classification. If every classification bin fits very poorly, then the best fit is not necessarily a good fit (Muthukrishna et al., 2019).

DASH makes use of the *rlap* ranking system, presented originally for the transient classifier SNID (Blondin & Tonry, 2007), as an additional test for quality in a classification. *rlap* is the product of the correlation scale height ratio,  $r$ , and *lap*, an overlap parameter.  $r$  is defined as the ratio between the highest normalised cross-correlation peak,  $h$ , and the root-mean-square (RMS) error of the anti-symmetric component of the cross-correlation product  $\sigma_a$ :

$$r = \frac{h}{\sqrt{2}\sigma_a} \quad (7)$$

*lap* is the overlap in  $\ln(\lambda)$  space between the input and template spectra. A larger *rlap* value indicates more similarities between the input spectrum being classified and the template it is being compared to. Hence, larger *rlap* values indicate a better quality classification.

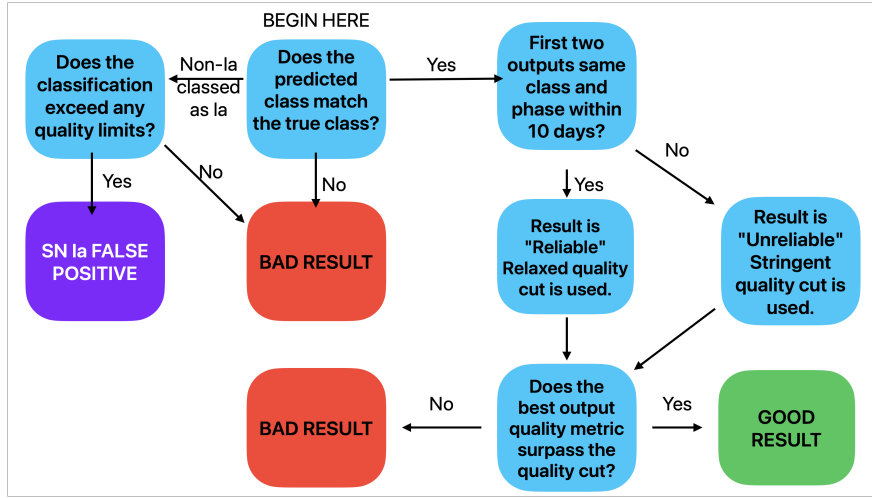


**Figure 5.** A flow chart illustrating the logic path for determining the quality of classifications. It follows the same path as that described in Section 4.

**Table 2.** The SN Ia and non-SN Ia transient subclasses for each classifier. The non-SN Ia transient subclasses included here match the various non-SN Ia input classes listed in Table 1. Any output classifications not included in this Table would be considered a misclassification if returned by a classifier.

Classifier	Binary Class	5 Classes	Corresponding Outputs
DASH	SNe Ia	SNe Ia	Ia-norm, Ia-91T, Ia-91bg
.	SNe Ia-pec	SNe Ia-pec	Ia-pec, Ia-csm, Ia-02cx
.	non-SN Ia	SNe Ibc	Ib-norm, Ib-pec, Ic-norm, Ic-broad
.	.	SNe II	Ib, IIP, II-pec, IIL, IIn
.	.	SLSNe	-
.	.	non-SN	-
NGSF	SNe Ia	SNe Ia	Ia-norm, Ia 91bg-like, Ia 91T-like, Ia 99aa-like
.	SNe Ia-pec	SNe Ia-pec	Ia 02es-like, Ia-02cx like, Ia-CSM-(ambiguous), Ia-pec Ia-CSM, Ia-rapid, Ca-Ia, super-chandra
.	non-SN Ia	SNe Ibc	Ibn, Ib, Ic, Ic-BL, Ic-pec, IIB
.	.	SNe II	II, II-flash, IIn, IIB-flash
.	.	SLSNe	SLSN-II, SLSN-IIn, SLSN-I, SLSN-Ib, SLSN-IIB
.	.	non-SN	TDE H, TDE He, TDE H+He
SNID	SNe Ia	SNe Ia	Ia, Ia-norm, Ia-91T, Ia-91bg, Ia-99aa
.	SNe Ia-pec	SNe Ia-pec	Ia-csm, Ia-pec, Ia-02cx
.	non-SN Ia	SNe Ibc	Ib, Ib-pec, Ib-norm, Ic, Ic-norm, Ic-pec, Ic-broad, IIB
.	.	SNe II	II, IIL, IIP, II-pec, IIn
.	.	SLSNe	SLSN, SLSN-I, SLSN-Ic, SLSN-IIn
.	.	non-SN	TDE, NotSN, AGN, LBV, M-star, QSO, C-star Ca-rich, ILRT, LRN

DASH returns an *rlap* value for each classification bin and an overall one for the fit. The overall *rlap* value is the weighted mean of all *rlaps* that reach some minimum threshold value defined by the user (default value of 6).

DASH has four modes of operation defined by its ability to fit or not fit transient host galaxies and its ability to use or not use known redshift values. We only make use of the known and unknown redshift modes. In the unknown redshift mode, the redshift is estimated by maximising *rlap* in redshift space. Host fitting leads to an increase in the number of output classification bins as each output now has a host class attached to each output. This increase in output bins leads diluted softmax percentages on outputs. The host fitting mode also doesn't function without redshifts provided. For this reason we do not investigate it.

#### 4.1.2 Determining Good DASH Classification

DASH presents several parameters with each classification in the Softmax probability and *rlap*. We will investigate both separately to see if a minimum threshold in either leads to higher efficiencies or purities in the sample following classification.

As mentioned in Section 4, our focus is in obtaining a pure sample of SNe Ia. Hence, we aim for 95% purity first. High efficiency is a secondary priority.

In Fig. 6 we classify the quality control sample (see Section 2.2) while iterating through different values for a cut on the Softmax probability. Also shown is the same process but iterating over potential *rlap* cuts.

It should be noted that currently the phase of the classification does not factor into how we judge the quality of the classification. Additionally, any classifications where the best-fitting class is the correct class, but the additional quality criteria are not met, are also considered 'other' classifications. While we know that the correct



class was selected, in the fitting of a real transient this classification would not be included in the final sample.

Due to our focus on obtaining a high-purity SN Ia sample for the purposes of cosmology, we must account for contaminants. This is the case where a non-SN Ia input spectrum is misclassified as a SN Ia, but otherwise is a successful classification. In a real sample, we would include this transient erroneously in our final SN Ia sample. Again, our logic in identifying contaminants is summarised visually in Fig. 5.

The number of SNe we expect to obtain from 4MOST is orders of magnitude larger than previous surveys such as Australian Dark Energy Survey (OzDES, Yuan et al., 2015) or the SuperNova Legacy Survey (SNLS, Astier et al., 2006). As such we can afford to slightly reduce the efficiency in classifying SNe Ia and non-Ia transients in the name of improving the purity of our sample by limiting the rate of contaminants.

In Fig. 6 we investigate the ability of the two main quality metrics in DASH,  $rlap$  and Softmax percentage, to improve the purity. It can be seen in Fig. 6a that there is no point where the purity drops below 95%. In fact the purity is close to constant at a value of 97.9%, only decreasing slightly at very high Softmax requirements where it is driven by a lack of good SN Ia classifications rather than increasing contaminants.

In Fig. 6b, we see the SN Ia and non-SN Ia efficiencies reduced very quickly as the minimum  $rlap$  requirement on classification is increased. However, similar to Fig. 6a, we see that the purity is stable as we increase the  $rlap$  requirement on classification. Only at high  $rlap$  thresholds do we see the purity improve, at which point the classification efficiencies (especially of non-SN Ia transients) is very poor. In fact, in the case where no  $rlap$  threshold is imposed we obtain the best result. This, of course, is identical to the result obtained by imposing no Softmax probability cut and returns classification rates for SNe Ia, non-SN Ia transients and contaminants at 78.3%, 70.0% and 2.1%, respectively.

Since we cannot improve upon these rates by imposing quality cuts on either metric, we will proceed with no quality thresholds imposed on classification. As such we make no use of DASH's built-in Reliability metric mentioned previously. This could be used to subject reliable results to a less stringent quality metric, but since we accept all classifications for DASH at face value, there is no use for it here.

There are some concerns that must be kept in mind if DASH is to be used as a mechanism to classify transients. For example, while DASH is user-friendly, fast-working and produces pure samples, it does so somewhat at the cost of user power. Compared to SNID or NGSF (Howell et al., 2005) the user's options are fairly limited. There is no front-end mechanism to pass an error function for weighting the fit or removing wavelength ranges with known contaminant features.

Additionally, and very importantly, the potential SN classes available for classification are somewhat limited. DASH can classify SNe Ia and common CC SNe like Ib/c, II, IIn and IIP. However, no other classes are included in its training sample and so other classes in the population simulations such as SLSNe, TDEs, and CaRT cannot be classified. They are either 'other' results or contaminants. Some of these transient classes are fairly exotic and rare, but there are many SLSNe in the simulation and for DASH they can only act as a source of contaminant classifications.

## 4.2 Next-Generation SuperFit

### 4.2.1 Using NGSF

Next-Generation SuperFit (NGSF) is a template matching SN classifier. Written in python, it is based on the Superfit classification package written in IDL (Howell et al., 2005). NGSF requires a set of transient and host templates to compare to the spectrum being classified. We use the updated template set recommended in the source<sup>3</sup>. The input spectrum is sequentially compared to each of these templates while iterating through a variety of redshifts, reddening corrections and different levels of host contamination for a variety of morphologies. The redshift and reddening arrays that are checked are defined by the user. Each spectrum being fit must be compared to every template at every possible combination of reddening and redshift and for every host galaxy. As a result, the classification time required varies significantly with how fine the redshift sampling is (Goldwasser et al., 2022).

NGSF returns its classification in the form of a reduced  $\chi^2$  value for each host, template, redshift, reddening combination. Input spectra are binned to match the templates and then a  $\chi^2$  value is obtained using the equation (reproduced from Howell et al. (2005)):

$$\chi^2 = \sum \frac{[O(\lambda) - aT(\lambda; z)10^{cA_\lambda} - bG(\lambda; z)]^2}{\sigma(\lambda)^2} \quad (8)$$

where  $O$  is the input spectrum,  $T$  is the transient template spectrum,  $G$  is the host galaxy template spectrum at a given redshift,  $z$ ,  $\sigma(\lambda)$  is the error on the input spectrum and  $A_\lambda$  is the reddening law.  $a$ ,  $b$  and  $c$  are constants that are varied during the classification process to check the template fit at varying reddening levels and at varying levels of host contamination. NGSF uses the reddening law of Cardelli et al. (1989). The closer to unity a template's  $\chi_{red}^2$  is, the more similarities there are between input spectrum and template. So the closest chi-squared to unity is considered the best-fitting template. As NGSF also iterates through different levels of host contamination for each template it returns the estimated galaxy fraction of the best-fitting templates. Since our spectra have known SN and host magnitudes in the fibre, this has potential as another method to judge classification quality.

The throughput in the simulated 4MOST spectra drops below 70% approximately below 4000 Å and above 8000 Å. We chose to limit the NGSF template comparisons to this wavelength range. In the case where the input spectrum has no attached error spectrum, NGSF has several options for generating error spectra which can be used as weights to calculate a reasonable  $\chi_{red}^2$  for the input. It can determine a linear error spectrum or a Savitzky-Golay (SG) (Savitzky & Golay, 1964) error spectrum. However, since the ETC generates error spectra, we use these for calculating  $\chi_{red}^2$ .

### 4.2.2 Determining Good NGSF Classification

The overall process for determining whether a classification is good is very similar to that for DASH, but replacing Softmax percentage or  $rlap$  with  $\chi_{red}^2$ .

NGSF has a variety of built-in mechanisms for calculating the error spectrum used in determining the  $\chi_{red}^2$  value for a given classification. Using a pre-existing error spectrum that is attached to the input spectrum is the intended mechanism, with the linear and SG error spectra options only intended to generate reasonable  $\chi_{red}^2$  values

<sup>3</sup> From the WISeREP repository

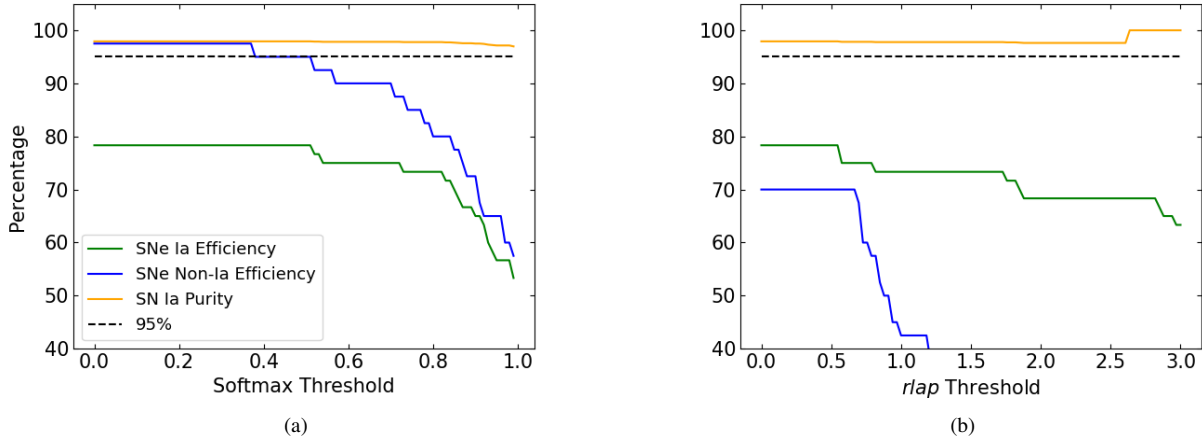


**Figure 6.** The effect of varying quality thresholds on DASH’s efficiency in classifying SNe Ia, non-Ia transients and the purity of the output SN Ia classifications using the quality control sample discussed in Section 2.2. The classification is performed with redshift priors provided. Panel a) shows this process as the softmax threshold varies and panel b) as the  $rlap$  threshold varies. No  $rlap$  threshold is imposed while Softmax percentage is investigated and vice versa. The dashed line marks a purity of 95%. It can be seen that the FDR is relatively stable with respect to any quality threshold imposed.

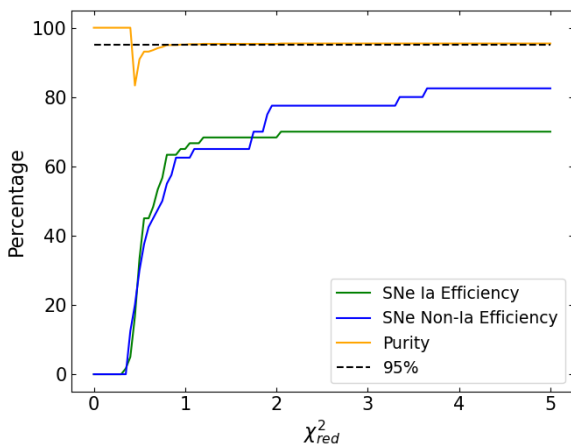


**Figure 7.** The percentage SN Ia efficiency, non-SN Ia efficiency and purity in green, blue and orange, respectively, for NGSF fitting the quality control sample while using attached error spectra. Redshift information was used in the classification. The dashed black line represents our 95% purity target. As in Fig. 6, we find that the purity is quite stable as the  $\chi^2_{red}$  limit is changed.

in the absence of an attached error spectrum. In Fig. 7 we investigate the potential of determining the quality of the NGSF classification using  $\chi^2_{red}$  with attached error spectra.

We find that the purity stabilizes as the maximum allowable  $\chi^2_{red}$  increases. The purity levels off at 95.8%. Similarly, at  $\chi^2_{red}$  limits of roughly 4, we see the SN Ia and non-SN Ia efficiencies level off as well at 70.0 and 74.2%, respectively. As we report with DASH, since classification rates stabilize or improve as quality cuts are relaxed, there is little reason to impose a quality cut using  $\chi^2_{red}$ . As such we decide to proceed without imposing a quality cut on NGSF classifications.

While NGSF returns no other parameters explicitly for assessing the quality of classification, it also estimates the ratio of transient flux to host flux, a value that we know from the simulation and that

we should be able to obtain from photometry during real 4MOST and LSST operations. Unfortunately, this does not seem to be good for identifying successful or unsuccessful classifications. We see from Fig. 8 that reducing the acceptable difference between true and predicted transient flux fraction does indeed increase the SN Ia purity. However, in order to increase the purity to over 95% we must set such a strict limit such that the SN Ia and non-SN Ia efficiencies are less than 20%. Similarly, in Fig. 8b, we see that there is significant scatter in the predicted transient flux fraction from the true value. We discard the idea of using the transient flux fraction as a mechanism by which to judge classification quality.

However, we also acknowledge that, since we should have access to photometry and thus should know fraction of galaxy flux in the spectrum, that this information could be used as a prior to constrain the classification.

NGSF has several distinct advantages over DASH, mainly in the form of user control. For example: the ability to set a redshift or reddening constant *range* with specified values or the capacity to exclude noisy wavelength ranges.

The final, and perhaps most considerable advantage, is NGSF provides easy access to the set of templates it uses. This makes it very easy to update the templates manually to include more examples of existing subclasses or new subclasses altogether. Updates to either require no additional training time, which would be needed to change the templates used by DASH.

## 4.3 Supernova Identification

### 4.3.1 Using SNID

SNID is an algorithm for determining the properties of a SN spectrum (Blondin & Tonry, 2007). It makes use of cross-correlation techniques and template matching to find best-fitting redshifts, ages and types for input templates.

We use templates collected from various samples by Kim et al. (2022), where a more complete description can be found. SNID is the origin of the  $rlap$  quality parameter that is explained in more detail in Section 4.1.1. Restated simply, input spectra are cross correlated in redshift parameter-space with SNID’s templates. The strength of

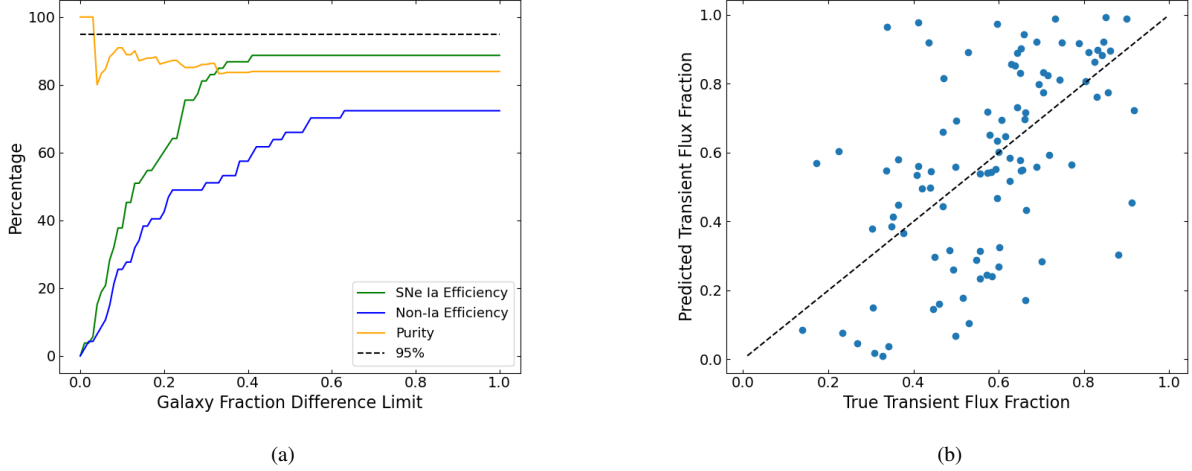


**Figure 8.** a) The percentage SN Ia efficiency, non-SN Ia efficiency and SN Ia purity when using the difference in host–transient flux ratios between the true values from our simulated spectra and the NGSF predicted value. The 95% purity target is represented by the dashed line. We can see that SN Ia and non-SN Ia classification rates can be good, but purity is very low. b) The NGSF predicted transient flux fraction against the true value. The dashed line represents a flux ratio of unity, or a correct prediction of transient flux fraction. It can be seen that there is significant scatter between the true and predicted values of transient flux fraction.

the cross correlation and the overlap in wavelength space leads to *rlap*, which gauges the quality of a classification. Classifications were performed over the same 4000 - 8000Å range as NGSF.

#### 4.3.2 Determining Good SNID Classification

The general philosophy for determining a good fit remains unchanged from our methods for NGSF and DASH. We check that the predicted best SN subclass is a subclass of the true SN class of the input. Then we may apply some form of quality cut to the classification to remove spurious classifications in the pursuit of reducing the FDR. SNID returns an *rlap* value alongside each classification and so this is the metric we will apply a quality cutoff to.

With SNID we make use of a reliability metric. DASH provides a reliability metric by default, with a classification deemed reliable if the top two classification bins share a subclass and are in adjacent phase bins. For SNID we perform an equivalent check: that the top two output classifications agree on subclass and that the phases are within 10 days of each other. Reliable classifications are subject to just 95% of the *rlap* limit determined in Fig. 9.

Fig. 9 shows the effect of different *rlap* quality thresholds on the SN Ia efficiency, the non-SN Ia efficiency and the purity. We see that an *rlap* of 3.7 is needed for the purity to rise above the dashed line at 95%, so this is the quality limit we will impose henceforth. We use this threshold rather than a higher *rlap* with better purities to avoid reducing our classification efficiencies.

This is quite a bit lower than the default of  $rlap > 6$  used in Muthukrishna et al. (2019) and the minimum acceptable value of  $rlap = 5$  used in Blondin & Tonry (2007). Although we do note continued improvements in the FDR at an *rlap* of 5.9, at this limit there has been significant reduction in the successfully classified SN Ia rate from 65.0% to 59.9%.

Unfortunately, requiring this minimum *rlap* results in the non-SN Ia efficiency dropping to a rate far below that of SNe Ia and similar results from previous classifiers, with only 30.0% of non-SN Ia transients being successfully classified as such. The majority of misclassifications either produced best-fits of SNe Ia, but with

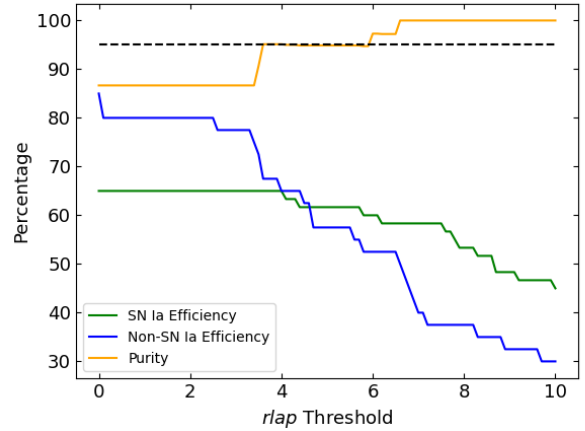


**Figure 9.** The efficiency per classification bin as a function of the *rlap* threshold for SNID. The dashed black line represents the 95% purity mark. The green, blue and orange lines denote the SN Ia efficiency, the non-SN Ia efficiency and the SN Ia purity, respectively. Again, the quality control sample described in Section 2.2 was used with redshift information provided. Unlike DASH and NGSF, the purity produced by SNID undergoes significant change as the quality threshold is varied. At  $rlap > 3.8$  the purity rises above 95%.

insufficient quality to be considered a contaminant, or as pure galaxy spectra, which are not considered a good non-SN Ia class (see Table 2).

As with NGSF, it is a significantly more powerful fitter than DASH with a large array of optional arguments that it can be passed to modify the fitting procedure as required. It has plotting functionality through the use of PGPLOT.

One advantage SNID has is the large variety of built-in transient classes and subclasses available for classification, as well as several morphologies of galaxy, AGN and a simple notSN classification amongst others that allow SNID to potentially identify non-transient

spectra. DASH and NGSF have no capacity to do this. NGSF can easily have new templates added, but DASH would require computationally expensive retraining for the same effect.

Further, addition of more subclasses is very simple. New templates can be added to the SNID repository provided they are in the correct format. Then the new classifications are added to a simple parameter file. In this paper we have 30 distinct classifications (a few SLSNe and non-SN classes were added to those that came built-in). However, SNID still seems to perform very poorly when classifying non-SN Ia spectra. This will be discussed further in Section 5.

One issue we encounter with SNID is that it occasionally fails to complete a classification and returns no output. In this case we assign a best-fitting classification of ‘None’ which is automatically determined to be an ‘other’ classification regardless of input class.

## 5 COMPARING CLASSIFIERS

We test each classifier both with and without redshift priors. Using redshift priors means that for each input spectrum we provide the classifiers with the true transient redshift as found in the input population simulation. In the case of using unknown redshifts we give no redshift information to DASH and SNID. NGSF is instructed to check redshifts between  $0 < z < 1.5$  with a sampling of  $\Delta z = 0.05$ .

The analysis in this Section makes use of the comparison sample of simulated spectra as described in Section 2.2. The constituent transient classes that make up this sample are found in Table 1.

### 5.1 Classification Efficiencies

We consider the binary and six-class classification schema shown in Table 2. This table lists the output classification from each classifier and indicates which classification they belong to in each schema. For the six-class scheme we make use of an ‘other’ classification bin. An ‘other’ output represents the case where an output classification does not meet that classifier’s quality threshold/limit or the case where an output classification has no corresponding input class. For example, we have no Ia-pec inputs and so can disregard a Ia-pec output as an ‘other’ classification. ‘other’ classifications are still considered for the purposes of calculating the classification efficiency of a given transient class.

We have two classification objectives as outlined in Section 1. First is the production of a SN Ia sample for cosmology. It is critical that this sample have a very high purity, even at the cost of efficiency. Second, we want to be able to provide live classification across several broad transient classes. In this case we still want high purity, but less so than in the SN Ia sample. A balance between high purity and efficiency is desirable.

#### 5.1.1 Binary Classification

The results of the classification of our host-contaminated spectra using the binary classification are shown in Table 3. For SNID we still require that a good classification must have  $rlap > 3.7$ .

We see that our DASH results, both with and without redshift priors, have very impressive purities well above our target threshold of 95%. Additionally, the SN Ia efficiency is fairly good with redshift priors, but it falls to just above 50% without. This is the largest drop in performance upon the removal of redshift information among the three classifiers by a significant margin. The non-SN Ia efficiency is significantly higher than that for SNe Ia, with redshift priors and it sees a much smaller drop when redshift priors are removed.

**Table 3.** The classification efficiencies of SNe Ia and non-SN Ia transients in the binary schema, and the purity of SNe Ia for each of the three classifiers. All three are tested with and without redshift priors provided to them.

Classifier	Ia Efficiency	non-SN Ia Efficiency	Ia Purity
DASH, known z	0.763	0.976	0.981
DASH, no z	0.517	0.914	0.970
NGSF, known z	0.781	0.957	0.983
NGSF, no z	0.653	0.896	0.936
SNID, known z	0.669	0.693	0.941
SNID, no z	0.558	0.709	0.832

However, around 30% of the successful classifications of non-SN Ia are the result of transients being classed as Ia-pec subclasses, as these are not considered Ia in the binary classification. Often these are non-SN Ia transients with Sc-type hosts. The narrow emission lines from the host are misinterpreted as circum-stellar medium (CSM) interaction, leading to a Ia-csm classification. This effect is also present in NGSF and SNID, but to a lesser extent.

NGSF outperforms DASH with redshift priors with a SN Ia classification efficiency and a purity that are marginally better than DASH’s and a non-SN Ia classification efficiency that is much better. When removing redshift priors we see a loss of performance across all three parameters. The loss in SN Ia classification efficiency is far less than that seen in DASH, and since the loss in non-SN Ia classification efficiency is similar, both rates remain better than those presented by DASH. However, we also see the purity falling to under 95%. Again, many misclassifications are Sc hosts being output as Ia-csm, although there are far fewer misclassifications in total.

SNID has a much lower SN Ia efficiency than DASH and NGSF when given redshift priors, and with these removed its performance with respect to SN Ia efficiency and purity gets worse. In all scenarios we see SNID produce the lowest efficiencies and SN Ia purities. Despite being low compared to DASH and SNID, SNID’s non-SN Ia efficiency is even more inflated. As well as galaxy emission features leading to erroneous Ia-csm classifications, SNID also has several non-transient classification bins. A significant number of the good non-SN Ia classifications are highly contaminated spectra being classified as ‘gal’. It should be noted that SNID was intended to have significant human oversight in classification, so relatively poor results under complete automation are not unexpected.

Between DASH and NGSF it is hard to choose the superior classifier. Performance is nearly identical with redshift priors. Without redshift priors there is a judgement call to be made between DASH’s lower SN Ia efficiency and NGSF’s lower purity.

The fact that purity always decreases when redshifts are not known, despite the naive expectation that the rate of Ia and contaminant classification should decrease commensurately, indicates systematic issues with the template/training sets across our classifiers. In every case they are dominated by SNe Ia. This may lead to DASH over-weighting features learned from SNe Ia templates, resulting in an increased likelihood that a Ia will be DASH’s top classification. Similarly, SNID and NGSF, when the input does not match well with any of their templates, and lacking a redshift to help discount templates, are most likely to find a SN Ia template as the best match as SNe Ia are the majority of their template banks.

More detailed discussion on how input SN Ia templates are being classified by DASH, SNID and NGSF can be found in the appendix, in Fig. A1. Similarly, more detailed discussion on the origin of contaminant classifications for each classifier can be found in Fig. A2.



### 5.1.2 5-Class Classification

Table 4 shows the comparison sample being classified with the non-SN Ia transient output bin divided into SNe Ibc, SNe II, SLSNe and non-SN transients. The efficiency recorded for SNe Ia and contaminants are unchanged, as the output bins are unchanged. However, we do see some finer detail about each classifier’s ability to classify CC SNe and non-SN transients. This is particularly relevant for judging a classifier’s ability to perform live TiDES classification across a range of different transient classes. Confusion matrices for the case with known redshifts are shown in Fig. 10(a).

It becomes apparent that DASH is reasonably successful at classifying SNe Ibc when redshift priors are provided, but is far less successful at classifying type II SNe. Unlike what we see in its SN Ia efficiency, when redshift priors are removed, there is not much change in performance for Type II SNe. The Ibc classification efficiency actually improves slightly, while the Type II classification efficiency decreases, but by far less than that of the SNe Ia. It cannot be stated strongly enough that DASH lacks all capacity to classify SLSNe and the various non-SN transients. Indeed, in Section 5.2, all combinations of classifiers that include DASH are incapable of successfully classifying any SLSNe or non-SN input spectra.

Despite the very strong results for non-SN Ia transients in the binary schema, NGSF produces quite poor results when we subdivide into the 5 class schema. The Ibc and II classification efficiencies are around 50% with redshift priors and both see a drop in performance when these are removed. The non-SN transient efficiency is very poor, hovering around just 10% with and without redshift priors. The only particularly strong result is the correct classification of 77.7% of SLSNe when redshift priors are provided. This is much better than SNID, which classifies less than 10% of input SLSNe correctly, and DASH which, as mentioned previously, cannot classify them. NGSF’s SLSN classification efficiency without redshift priors is far lower than that for CC SNe at just over 20%.

As expected from the poor non-SN Ia efficiencies reported in the binary schema, SNID produces poor classification efficiencies of all non-SN Ia transient subclasses in the 5-class schema. A large number of non-SN transients are classified as ‘Gal’ or a galaxy template by SNID. While this is indeed a non-SN classification, it is not a transient classification and as such leads to an ‘other’ classification (hence this classification does not appear in Table 2).

## 5.2 Using Multiple Classifiers at Once

For both live classification of transients and when creating SN Ia samples for cosmology, it is critical to limit contamination in the output sample. For live classification, this is important for all SN classes. For cosmology, it only matters that the SN Ia sample is of high purity, even to the detriment of the SN Ia efficiency. This is particularly true given the very large number of transients that 4MOST is expected to observe. Table 4 shows that individual classifiers struggle to limit contamination in the output SN Ia sample and are poor classifiers of even broad non-Ia SN classes. The obvious question is: what is the result of combining the classifications from different classifiers for each transient?

To answer this, we consider the six-class schema first described in Section 4. In order to mimic the classification of a real sample, any input spectrum that does not meet the quality cut for a classifier is considered an ‘other’ output and is not included in our final sample of classified spectra. Additionally, Ia-pec classifications and other non-SN Ia outputs that do not align with any input class will, by default, lead to an ‘other’ output.

We first investigate the effect of classifying spectra with all combinations of two out of the three classifiers. In these cases, if both classifiers are not in agreement on the output classification, then the result defaults to an ‘other’ output regardless of the quality of either classification.

Fig. 10 shows that when using known redshifts, requiring two classifiers to agree has the effect of reducing the overall efficiencies for all five original output classes and a large increase in the number of ‘other’ outputs compared to the individual classifier results. However, we also see an increase in the purity of SNe Ia. The purity is now so high that we choose to disregard the *rlap* limit for SNID. We can afford the purity to decrease slightly to improve efficiency.

The extreme case for a combined classifier is to use all of DASH, NGSF and SNID simultaneously. The results for SNe Ia are shown in table 5. With the combination of all three classifiers, we now classify around 60% of all SNe Ia when redshifts priors are provided, but get very few successful classifications for any other input class. The sample of classified SNe produced by this combined classification is acceptable assuming that we are only interested in cosmology and care for nothing other than SNe Ia.

Without redshifts we report much reduced success. The non-SN Ia efficiencies remain around 10% or less and the SN Ia efficiency is nearly halved to 33%. This is very low compared to other combined and individual classifiers, but with the benefit that the purity is very close to 100%. It remains to be determined where exactly the optimum balance lies between pure SN Ia samples and large SN Ia samples for the purposes of cosmology.

While the efficiencies for non-SN Ia classes are very poor, there is some potential for high purity. Using all three classifiers, 87% of SNe II are misclassified as ‘other’ or SNe Ibc. However, in this case the purity of output SN II sample is very high despite the low classification efficiency. In fact, by using a combined classifier consisting only of DASH and SNID we retrieve some of the classification efficiency, classifying just under a third of SNe II successfully to produce a sample that is 96.4% pure.

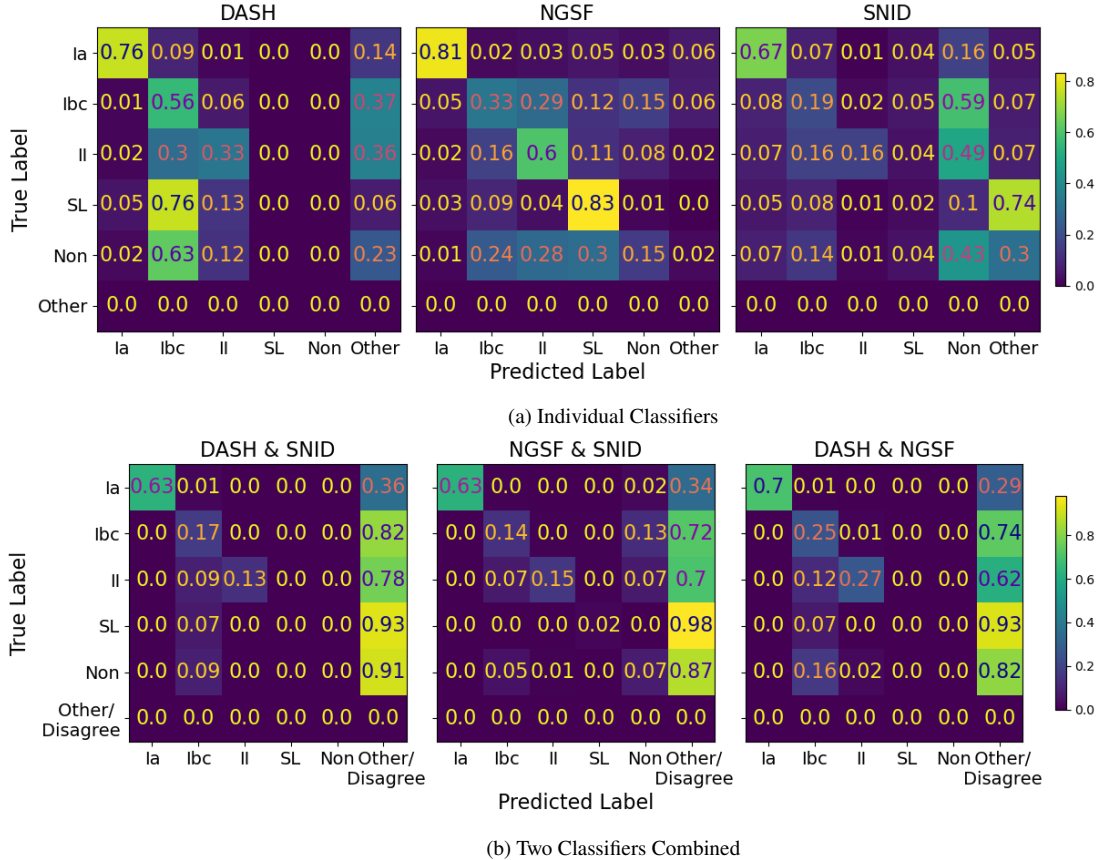
Regarding the other non-SN Ia classes: SNe Ibc are overwhelmingly classified as failed, ‘other’ classifications. Additionally, we see significant contributions to the contamination in the SN Ibc class from SNe II and the non-SN transients. Due to DASH’s presence in this combined classifier, the classification efficiencies of SLSNe and non-SN transients are zero. Indeed this can also be seen in Fig. 10, in both double classifier combinations including DASH.

The poor classification efficiencies shown in Fig. 10(b) and Table 5 suggests that the use of combined classifiers alone is not particularly appropriate for live transient classification. However, it does indicate the potential for very pure SN Ia and SN II samples, although the latter sample has very low classification efficiency. As such, combined classifiers could still form an important part of a live classification plan. A combined classifier could be used as a first classification step to remove this high purity SN Ia sample prior to additional, later classification steps. Depending on the classifier used, this can also be done for the very pure (but inefficient) SN II sample produced. We investigate the potential for a second stage of classification in Section 5.3.

We conclude that there are two reasonable options for the best combined classifier. Either DASH and NGSF or all three classifiers combined. Our recommendation is the use of just NGSF and DASH. The improvement in SN Ia and SN II efficiencies between DASH and NGSF and using all three is 10% or more. This amounts to the addition of hundreds of transients into the final sample at the cost of doubling an already negligible non-SN Ia contamination.

**Table 4.** The efficiency for classifying SNe Ia, SNe Ibc, SNe II, SLSNe, non-SN transients and FDR for each classifier.

Classifier	Ia Efficiency	Ibc Efficiency	II Efficiency	SL Efficiency	non-SN Efficiency	Ia Purity
DASH, known z	0.763	0.665	0.388	0.0	0.0	0.981
DASH, no z	0.517	0.678	0.310	0.0	0.0	0.970
NGSF, known z	0.781	0.485	0.549	0.777	0.095	0.983
NGSF, no z	0.653	0.435	0.342	0.233	0.115	0.936
SNID, known z	0.669	0.193	0.165	0.023	0.014	0.941
SNID, no z	0.558	0.275	0.149	0.082	0.027	0.832

**Figure 10.** Confusion matrices showing the results for a) the three individual classifiers and b) all three combinations of two of the three classifiers working simultaneously. The ‘other’ output classification is reserved for those spectra which do not meet the quality cuts of the classifier(s) being used, output classifications with no corresponding input class and, in the case of the combined classifiers, an input spectrum that causes the two classifiers to disagree on the output class. Classification was performed with redshift priors provided in all cases. Totals have been normalised by true label (by row). High efficiency and purity samples would be indicated by high concentration along the matrix diagonal. Horizontal scatter indicates loss of efficiency, vertical scatter indicates loss of purity.**Table 5.** The SN Ia efficiency and purity for all possible combinations of two or three classifiers. Successful classification requires a SN Ia output from all involved classifiers. No classifiers have individual quality cuts imposed.

Classifiers	Redshift	Ia Efficiency	Ia Purity
DASH & NGSF	Known	0.700	0.9995
NGSF & SNID	.	0.640	0.9962
DASH & SNID	.	0.645	0.9969
ALL	.	0.610	0.9998
DASH & NGSF	Unknown	0.429	0.9986
NGSF & SNID	.	0.426	0.9804
DASH & SNID	.	0.396	0.9896
ALL	.	0.330	0.9996

### 5.3 Potential Photometric Cuts

Individually, we see mixed results from the classifiers. Depending on the classifier and redshift information used, efficiencies can change by up to 50% and SN Ia purities by as much as 15%. From a cosmology perspective we obtain both high-purity and reasonably high efficiency in SN Ia classification from DASH and NGSF, but only when redshift information is known, and it is yet unclear to what extent prior redshift information will be available for TiDES transients.

From a live classification perspective, there appears to be no single classifier from which we can expect a reasonable classification efficiency across the SN Ibc, II, SL and non-SN classes. Additionally we do not even consider the classification purity in these classes or any potential desire to perform classifications on finer classes than the five coarse classes investigated so far.

To this point we have attempted classification on every transient

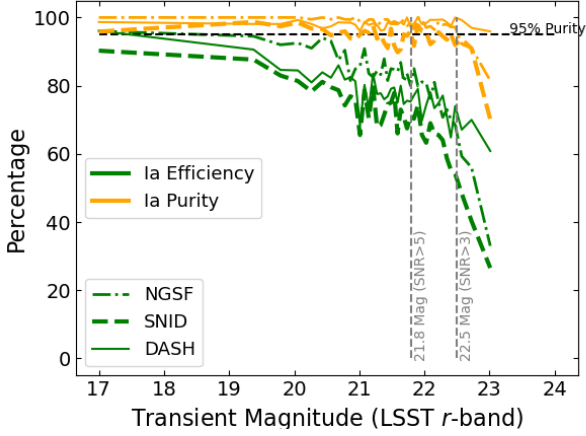


**Figure 11.** The SN Ia purity (orange) and efficiency (green) as report by DASH, NGSF and SNID as a function of the true transient magnitude. The SNe Ia are in magnitude bins of 200 transients, with each plotted point at its bin’s centre. The 95% purity target is marked by a black dashed line. Two potential transient magnitude cuts are marked by grey dashed lines at 21.8 and 22.5 mag. We find that these limits roughly correspond to efficiency dropping below 80% and purity falling below our 95% target, respectively.

that has received any exposure time in the survey simulation. We will now investigate two obvious sources of ‘other’ classification to see if applying cuts to the sample prior to classification will improve results. In Section 5.3.1 we investigate making cuts on the fraction of fibre flux deriving from the transient (as opposed to its host galaxy) and in Section 5.3.2 we investigate cuts based on the brightness of the transient. Both of these quantities should be reasonably obtainable from the LSST photometry that TiDES will use to flag potential transient targets.

### 5.3.1 Apparent Transient Magnitude

The most obvious sample cut that can be introduced from photometric information is a cut on transient magnitude. In this section we investigate the potential for applying a cut to our transient sample based on the  $r$ -band magnitude of the transient. This magnitude should be obtainable from the LSST-derived data that triggers a transient observation by 4MOST-TiDES in the first place, making it feasible to use for live classification.

Fig. 11, presents the efficiency and purity of SN Ia classification for all three classifiers. It also proposes two potential values for a transient magnitude cut to our sample. These values, 21.8 and 22.5 mag, are derived in Frohmaier et al. (in prep.) as the magnitudes that correspond to transient signal-to-noise ratios (SNRs) of 5 and 3, respectively, where SNR is calculated as the average in 15 Å bins between 3,500 and 8,000 Å. Indeed Frohmaier et al. (in prep.) reports the SNR = 5 threshold as the conservative minimum to meet TiDES’s spectral success criteria, with the SNR = 3 limit a more optimistic estimate based on the work of Balland et al. (2009). Here, we find that these SNR cuts of 5 and 3 correspond roughly to the SN Ia efficiency falling below 80% and the purity falling below our 95% threshold, respectively.

In Table 6 we present the results from our 5 class classification schema as in Table 4, but now with the effects of cutting transients fainter than 21.8 and 22.5 mag. This does significantly reduce the final sample size, by up to 45% for the stricter 21.8 mag cut. However,

Classifier	$r$ -band Cut	Ia Eff.	non-Ia Eff.	Ia Pur.
DASH, known $z$	21.8	0.801	0.740	0.980
	22.5	0.781	0.705	0.983
	None	0.763	0.691	0.981
DASH, Unknown $z$	21.8	0.673	0.737	0.970
	22.5	0.567	0.703	0.972
	None	0.517	0.688	0.970
NGSF, Known $z$	21.8	0.877	0.953	0.993
	22.5	0.849	0.944	0.989
	None	0.781	0.910	0.983
NGSF, Unknown $z$	21.8	0.704	0.846	0.967
	22.5	0.684	0.815	0.957
	None	0.653	0.800	0.936
SNID, Known $z$	21.8	0.754	0.348	0.950
	22.5	0.718	0.319	0.948
	None	0.669	0.295	0.941
SNID, Unknown $z$	21.8	0.678	0.424	0.876
	22.5	0.589	0.398	0.857
	None	0.558	0.383	0.832

**Table 6.** The binary classification results of every combination of classifier and redshift prior. The full results of Table 3, with the full sample of observed objects, are reproduced with the magnitude cut recorded as None. Additionally, we report the same results, but with only transients brighter than  $r$ -band magnitude cuts of 21.8 and 22.5 mag. The final sample is reduced in size to 55% and 83% by magnitude cuts at 21.8 and 22.5 mag, respectively.

we generally see significant improvements across SN Ia efficiency, non-SN Ia efficiency and SN Ia purity. These improvements range from a 15% gain in SN Ia efficiency for NGSF without redshift priors to the DASH SN Ia purity remaining constant.

In particular, NGSF reports very good results with the 21.8 (SNR > 3) sample cut. Table 7 shows the more detailed results for NGSF with the 5 class classification schema with the 21.8 magnitude cut on the sample. Compared to the results in Table 4 we see that the cut significantly improves the efficiencies for NGSF for all transient classes with redshift priors provided, although it also worsens the efficiencies for all transient classes when these are not available.

In Section 5.2 we found that, while combined classifiers are very good at creating high purity, low efficiency SN Ia samples, they are poor classifiers of non-SN Ia classes. This makes them ineffective for TiDES live transient classifications. We also found in Section 5.1, that the individual classifiers produce mediocre efficiency and purity in most transient classes when operating on every transient observed in the 4MOST survey simulation. However, for TiDES transients brighter than  $r=21.8$  mag, NGSF appears to be a good choice for automated live classification.

However, this comes with several caveats. First, this is only true with robust redshift information. Second, this only applies with relatively broad transient classes. For example, NGSF often classifies Ib-norm inputs as SN Ic subclasses and vice versa. Finally, and perhaps most importantly, while the SNe Ia purity is high, the purity of the other classification bins can be far lower. For example the SN II purity is 78%, and the Ib-c purity is just 59%.

From the point of view of the potential cosmology sample of SNe Ia obtained in Section 5.2, cutting transients from our sample based on their apparent magnitudes has less impact on the purity than the efficiency. While NGSF and SNID see 2-4% improvement, DASH’s purity remains very close to constant. Compared to the needs of live classification, it is less clear if this small improvement in purity compensates for the significant fraction of the sample discarded before classification. In fact, applying the magnitude cut to the combined DASH-NGSF classifier reduces the SN Ia sample produced by over one third with redshifts. Although technically the efficiency of the

Redshift	Ibc Eff.	II Eff.	SL Eff.	non-SN Eff.
Known z	0.629	0.792	0.848	0.142
Unknown z	0.535	0.420	0.211	0.06

**Table 7.** The non-SN Ia efficiencies of NGSF with and without redshift priors, after limiting the sample to transients with  $r < 21.8$  mag. SN Ia efficiency and purity are unchanged from Table 6 and so are not listed. See Table 4 for the equivalent efficiencies with no apparent magnitude cut.

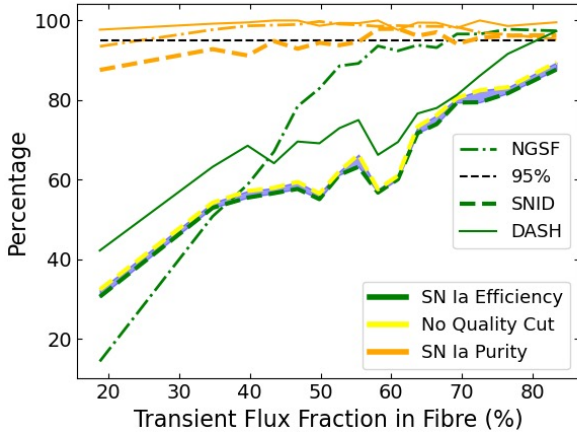


**Figure 12.** The SN Ia efficiency (green) and purity (orange) as a function of the fraction of the total flux in the spectrum that originates from the transient. The SNe Ia in our sample are grouped into bins of 500 transients by flux fraction. For SNID only: the shaded region indicates the range of potential SNe Ia efficiency that could be obtained by relaxing the  $rlap$  quality limit. The yellow line is the upper limit where no quality limit is placed on classifications. Redshift is known in all cases. All three classifiers produce similar trends in SN Ia efficiency and purity. In every case the classification efficiency and purity trend better as the transient flux fraction increases.

classified SN Ia sample increases from 70% to 77% with redshifts, this is a significant loss of sample size for a negligible change to purity.

### 5.3.2 Transient Flux Fraction

After transient magnitude, the second obvious source of classification error in our sample comes from high levels of host galaxy flux in our spectra. In this section we discuss the effectiveness of DASH, NGSF and SNID as a function of transient flux fraction, where the transient flux fraction is the fraction of the flux in a 4MOST fibre that originates from the transient. We report the potential to improve classification results by introducing a sample cut in transient flux fraction-redshift space.

We investigate using our 5-class classification schema as in previous sections, but also investigate the maximum SN Ia classification rate for SNID. The maximum SN Ia rate is the fraction of input SNe Ia that are classified as a SN Ia subclass by a classifier while completely ignoring all other metrics of quality on the classification. It represents the best case scenario for classifying SNe Ia in the case for efficiency where we are not concerned with the purity. We see in Fig. 12, that removing the  $rlap$  quality threshold for SNID classifications would result in only a few additional successful SN Ia classifications.

Generally, the trends in classification rates against the transient flux fraction are as one would expect. As the transient flux fraction increases (the spectrum’s host contamination is reduced) we see

improvements in the SN Ia efficiency and purity. The shape of these plots is very similar to those produced by transient magnitude binning in Fig. 11. The purity tends to approach our 95% threshold at transient flux fractions of 40 - 50% if it is not already above that threshold in the most contaminated bin. Fig. 12 indicates that all three classifiers have similar slopes in their purity with different initial values. Although not shown in the figure, the same trend was found without redshift priors, albeit with slightly larger values for DASH and much larger values for NGSF and SNID.

For SNID, the only classifier where we found it to be beneficial to implement a quality cut on output classifications, we see that the SN Ia efficiency without this quality cut tracks the efficiency with the cut very tightly. In fact, it appears that the quality cut removes a very small number of otherwise successful SN Ia classifications. Since the purity is poor, particularly when redshifts are not provided, it is possible that the quality cut is now reducing purity by cutting otherwise successful SN Ia classifications when our sample is scaled up to the full survey simulation. See Section 5.2 for a more detailed discussion of this.

We look at our results in flux fraction-redshift space in Fig. 13. At high redshift only transients that have bright absolute magnitudes, especially transients in the SLSN class, will be observed. So transient flux fraction is likely to be high as we are biased to intrinsically brighter transients while host brightness remains constant. However, we also expect the spectral features of our transients to be shifted outside of 4MOST’s wavelength range, making them harder to classify. Indeed the  $rlap$  classification quality parameter employed by DASH and SNID depends directly on the wavelength overlap between the input spectrum and matching template. We hope to find regions of this parameter space without contaminants or fewer misclassifications, where we could assign positive results a greater degree of certainty.

A few obvious points of interest are the trend to greater transient flux fractions with increasing redshift and the incidence of unsuccessful classifications of SNe Ia (orange histograms) beginning to drop off as the transient flux fraction surpasses around 40%. The SN Ia count histograms are fairly uniform for the three classifiers in the relative distributions of the successful and unsuccessful SN Ia classifications, but we see variation in the width of the successful classification histogram. In particular, there are obvious differences in the number of misclassified SNe Ia between the classifiers.

This plot also reveals one limitation of the binary classification schema. While reasonable from the perspective of investigating cosmology and SNe Ia, it indicates many successful classifications of SLSNe at high redshifts by DASH. In reality DASH has no capacity to classify SLSNe and so these are actually SLSN inputs being classified as other non-SN Ia transients such as SNe II or Ibc.

Also concerning are the clusters of SLSNe at high redshift that are classified as SNe Ia in all three classifiers. These SLSNe are being fit overwhelmingly as SNe Ia-91bg. This does lead to a potential mechanism for increasing purity. As can be seen in Fig. 13, the successful SN Ia classifications (and indeed instances of SNe Ia in general) drop off quite sharply after  $z = 0.60$ . Each classifier has contaminants beyond this redshift that could be dismissed out of hand if accurate spectroscopic redshifts for host galaxies are known.

For now, with the precise extent to which TiDES will have host redshift information, we do not implement such a cut. However, we make note of it and strongly encourage such a cut in the cases where redshifts are known.

An obvious location for a cut on the transient flux fraction is the point at which the good SN Ia classifications begin to dominate over misclassifications. This is the point where the histograms in Fig.



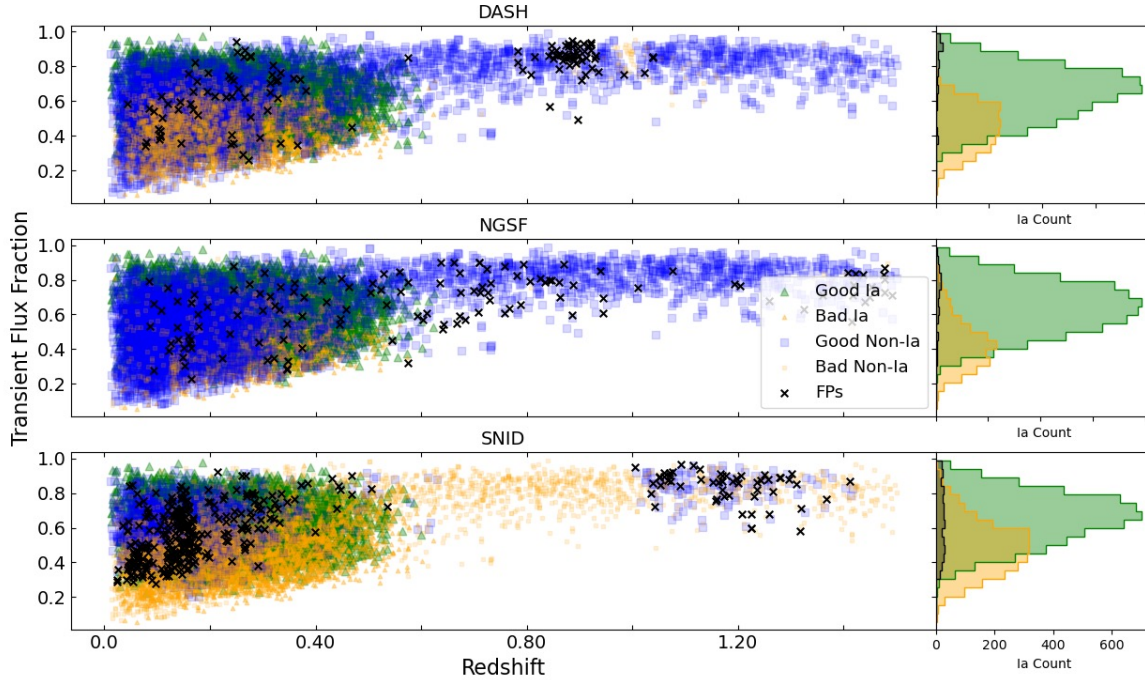


**Figure 13.** The classification results in the binary schema with known redshifts for all three classifiers in transient flux fraction-redshift space. Green, blue and orange points indicate good SN Ia classifications, good non-SN Ia classifications and failed classifications, respectively. The histograms show the counts of only SN Ia classifications and contaminants with the same colours. There are regions of the parameter space for each classifier where false positive SN Ia classifications cluster, often at high redshifts. We also see similar distributions for successful and unsuccessful SN Ia classifications.

13 show larger green bars than red. This occurs at a transient flux fraction of 0.38 for DASH, 0.38 for NGSF and 0.42 for SNID.

In Table 8 we present the results of our 5-class classification schema for NGSF as we employ a variety of different photometric cuts to the input sample. We see that using only a cut for transient flux fractions greater than 0.4 returns very similar classification results across all transient classes to the 21.8 transient magnitude cut employed in Section 5.3.1. However, this cut leaves 81.7% of the original sample compared to just 55.2%. We also find that better results are produced by the use of both cuts simultaneously, but this does significantly limit the sample size for classification.

However, we conclude that the best photometric cut for live classification is likely to be transient transient magnitude  $r > 21.8$ . While the sample size after the flux fraction cut is larger and the SN Ia efficiency is improved, the SN Ia purity and the efficiencies of other classes are worsened. Indeed, while not shown in Table 8, the purity of the non-Ia classes are worse under the flux fraction cut than the transient magnitude cut.

#### 5.4 An Example Classification Plan

In this final section we propose just one possible scheme that could be employed by TiDES for live classification of transients. The pipeline is illustrated by Fig. 14 and assumes redshift information is provided for all classifications. The pipeline consists of two separate classifications of the sample of transients. First, the full sample is classified by the combined DASH-NGSF classifier recommended in Section 5.1. This produces very pure samples of SNe Ia and SNe II although, particularly for the latter, with less good efficiency. The SNe Ia sample produced by this first classification step has 99.9% purity and should be appropriate for use in cosmology.

From the sample of spectra not classified by the combined classifier, we now take only those with a transient magnitude brighter than 21.8 mags as discussed in Section 5.3.1. These bright objects are then refit with just NGSF. This produces reasonably pure and complete samples of SNe Ibc and SLSNe. It also classifies a few additional SNe Ia and SNe II which can be combined with the existing samples to increase their efficiencies at the cost of their purities. The only class with poor results is the non-SN transients. Here we only classify 8.1% correctly and over 95% of the resulting sample is contamination from other classes. This is an issue with NGSF’s template bank and the absence of such spectra from DASH’s training set. When considered in full, the classification pipeline leaves almost exactly a quarter of transients unclassified.

This is a reasonably successful classification. It far outperforms any individual spectroscopic classifier that we have tested in this report. This classification scheme obtains a very pure SNe Ia sample for cosmology in addition to producing classification efficiencies and purities in non-SN Ia classes that are suitable for live transient classification.

It is worth noting that this is a very generalised pipeline plan. There is significant room for fine-tuning to specific science cases. For example, replacing the cut on transient magnitude to the cut on transient flux fraction as discussed in Section 5.3.2, the pipeline will produce samples with higher efficiencies at the cost of purity. Additionally the percentage of unclassified objects drops to just 18%. In this case the SLSN purity drops to around 65%, but this is compensated by an efficiency of over 80%.

Additional cuts from photometric information can be added to either stage of the pipeline to increase purity at the cost of efficiency. Different cuts than those discussed here can be used, which will effect

Cuts	Sample Size	Ia Eff.	Ia Purity	Ibc Eff.	II Eff.	SL Eff.	Non-SN Eff.
None	100%	0.781	0.983	0.485	0.549	0.777	0.095
$r$ -band Magnitude > 21.8	55.2%	0.877	0.993	0.629	0.792	0.848	0.142
Transient Flux Fraction > 0.4	81.7%	0.889	0.981	0.621	0.742	0.832	0.103
Both	47.7%	0.942	0.993	0.721	0.842	0.848	0.127

**Table 8.** SN Ia efficiency, SN Ia purity and the efficiencies of the non-SN Ia classes for NGSF with known redshifts depending on the photometric cuts employed. Noted for each cut is the percentage of the input sample that remains following the application of the cut(s). Efficiency is based on the transients in the classified sample, so objects removed by the photometric cuts do not contribute. Only NGSF is shown, having been identified as the most promising candidate for live classification

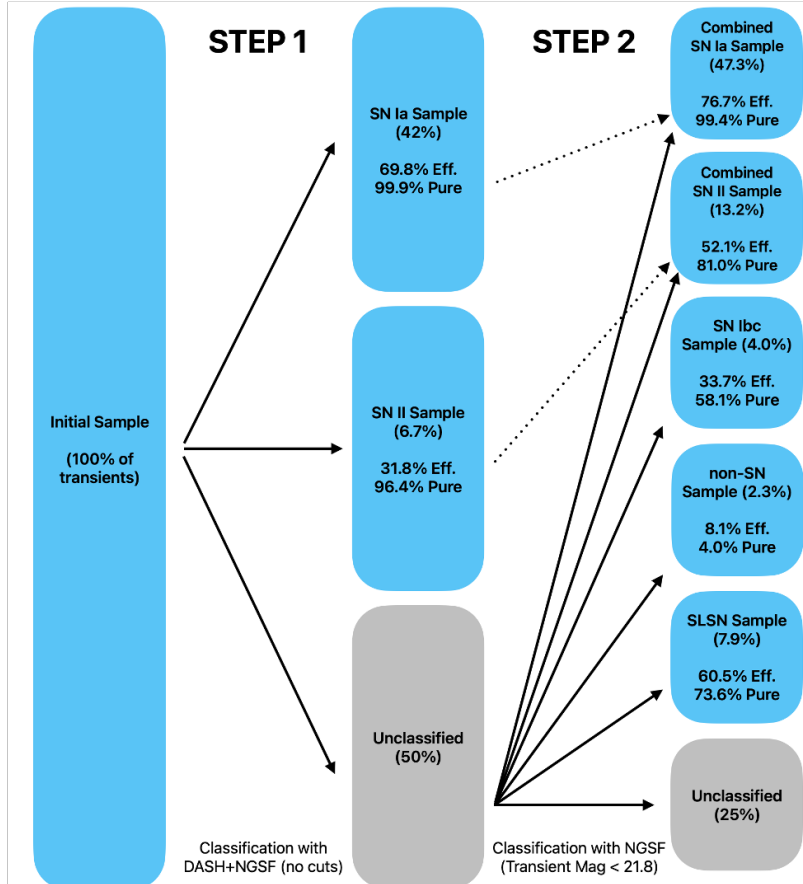


**Figure 14.** An example of a classification pipeline that could be employed by TiDES for the purpose of live classification of transients. The output samples of from each step in the classification pipeline are provided with their efficiencies and purities labeled. The samples of SNe Ia and SNe II provided after the second classification step represent the combination of the transients from the first classification and those from the second. Percentages of the total sample size are listed in brackets for each classes final sample. Classifications are performed with redshift information.

each class differently, allowing for parties interested in specific SNe classes to be specific in their classification.

The final advantage of such a classification model is that it is versatile and easily communicated to the community. By providing only: the class from the 5-class schema output by DASH and NGSF, the  $r$ -band magnitude of the transient and host near time of observation and the redshift of the system, it would be possible for members of the community to adjust the transient sample selected to suit their science goals.

#### 5.4.1 Comparison to Photometric Classification Results

In this subsection, we compare three recent photometric classification papers surrounding a recent photometric classifier and its use with the Dark Energy Survey (Möller et al., 2022).

Möller & de Boissière (2020) presents the photometric transient classifier SUPERNOVA classifying simulated light curves with spectroscopic redshift information and incomplete light curve information. Additionally, Möller et al. (2022) and Möller et al. (2024) present SUPERNOVA classification results on real light curves with and without host redshifts, respectively.

Specifically, Möller et al. (2024) presents the binary classification of DES 5-year data release SNe without any redshift information provided as a prior. When the light curves of transients being fit without redshifts are trimmed to only include photometry up to peak brightness, SUPERNOVA produces an accuracy, a Ia efficiency and a Ia purity of 90.46 %, 92.49 % and 91.93 %, respectively. By comparison, if operated as a binary classifier, our classification plan from Section 5.4 produces an accuracy, a Ia efficiency and a Ia purity of 80.70 %, 51.76 % and 97.03 %. Additionally, we can consider

only the high-confidence SN Ia sample produced by the combined NGSF-DASH classifier to improve the SN Ia purity to 99.86 % at the cost of reducing efficiency to just 42 %.

Möller et al. (2022) also applies SUPERNOVA to the photometric sample produced by the DES 5-year data release. This produces a cosmologically useful sample of 1,484 SNe Ia with spectroscopic redshifts. The predicted efficiency and purity of the sample are 98.51% and 97.73%, respectively. Again, we consider both the high-confidence SN Ia sample and the larger, less confident, SN Ia sample produced by our classification pipeline. Now with redshift priors, the less confident sample has an efficiency of 76% and purity of 99.5%. We can sacrifice some efficiency to improve purity and use the high confidence SN Ia sample produced by the combined DASH-NGSF classifier. This increases purity to 99.9% with efficiency just under 70%. Regardless of what redshift information is available, our classification plan produces a much purer SNe Ia sample, at the cost of lower efficiency and accuracy than SUPERNOVA.

While most photometric classifiers function purely in a binary (SN Ia v non-SN Ia) schema and with complete light curves, in Möller & de Boissière (2020), SUPERNOVA reports results using ternary and seven-way classification schema, similar to our 5-class schema.

SUPERNOVA reports an accuracy of 77.8% for its ternary schema (SNe Ia, Ibc and II) and 64.2% for the seven-way classification schema (SNe Ia, IIP, IIn, IIL1, IIL2, Ib, and Ic). In each case these are the accuracies expected from light curves consisting, on average, of 2.4 distinct nights of multi-colour observations up to 2 days before peak brightness. These percentages improve to 81.5% and 69.8% for an average of 3.1 distinct nights of multi-colour observations up to 2 days after peak brightness. All classifications also make use of spectroscopic redshifts.

For comparison our example pipeline, in the 5-class schema (SNe Ia, Ibc, II, SL and non-SNe), produces a comparable classification accuracy of 89.4%. Additionally, if we consider only SNe Ia, Ibc and II to mimic the ternary schema, we obtain an accuracy of 93.5%. From Frohmaier et al. (in prep.) the requirements to flag a transient for spectroscopic follow-up are 3 *griz* detections in two distinct nights, with the added requirement that at least one of these detections be brighter than 22.5 mag. We also assume spectroscopic redshifts are available. Our use of spectroscopy produces a roughly 15% improvement on the accuracies from photometry with similarly incomplete light curves.

## 6 CONCLUSIONS

In this paper we set out to determine whether the classification of transients discovered by 4MOST-TiDES can be automated using one or more spectroscopic transient classifiers. We want to know which classifier(s) are the best from a live-classification and cosmological point of view. To do this, we simulated realistic blended spectra using pre-existing simulations and the 4MOST ETC and classified them using DASH, NGSF and SNID.

The efficiencies of DASH, NGSF and SNID are lower than those reported in their original papers. This is the result of different quality data and fainter SNe, alongside significant host contamination. We find that, individually, NGSF produces the best efficiency for SN Ia classifications, although its non-SN Ia contamination is large if redshift information cannot be provided. None of the individual classifiers were robust enough to recommend their use for automated classification.

We find that the low purities in SNe Ia can be mitigated by using several classifiers at once and requiring an agreement between them

on each classification. This is costly for the SN Ia efficiency, but with the benefit of having vastly reduced contamination in the output sample. We get good results from a combination of DASH and NGSF, with SNe Ia efficiency of 69.8% and purity of 99.9%. Purity can be marginally improved by including SNID in the combined classifier, but at the cost of a much reduced efficiency.

This allows for the automation of SNe Ia classification and the production of good cosmology samples. However, it alone does not lead to a solution for general automated classification. The combined DASH-NGSF classifier struggles to classify SNe Ibc, II, SLSNe and non-SN transients.

We investigated a variety of photometric cuts that could be applied to our data to improve the resulting transient classifications. We found that only classifying those objects with transient *r*-band magnitudes brighter than 21.8 could significantly improve classification purity across all transient classes, but at the cost of classification efficiency. Similar results can be obtained by only classifying objects for which SNe flux comprises more than 40% of the flux within the observing 4MOST fibre.

We present an example classification plan. We show that a first classification of the combined DASH-NGSF classifier, followed by an NGSF classification run on all transients above the transient magnitude cut produced reasonable efficiencies and purities for all classes other than non-SN transients. We emphasize that such a classification pipeline is easily fine-tuned to specific science cases and conclude it is viable for live automated classification.

Finally, it is currently unclear to what extent 4MOST-TiDES will be able to obtain redshift information from host galaxies to be used in transient classification. The change in efficiencies and purities is significant between known and unknown redshifts and represents perhaps the largest uncertainty in the results of this paper. Work is currently underway investigating how consistently a redshift can be derived from features in blended host–transient spectra.

A future step in this work will be to optimize the classification scheme via end-to-end cosmological simulations, in order to show which combination of classifiers and photometric cuts minimize the uncertainty on derived cosmological parameters.

## ACKNOWLEDGEMENTS

AM gratefully acknowledges support from an STFC PhD studentship and the Faculty of Science and Technology at Lancaster University. IH gratefully acknowledges support from the Leverhulme Trust [International Fellowship IF-2023-027] and the Science and Technologies Facilities Council [grants ST/V000713/1 and ST/Y001230/1]. Y.-L.K. has received funding from the Science and Technology Facilities Council [grant number ST/V000713/1]. AM is supported by the ARC Discovery Early Career Researcher Award (DECRA) project number DE230100055. ET was supported by the Estonian Ministry of Education and Research (grant TK202), Estonian Research Council grant (PRG1006) and the European Union’s Horizon Europe research and innovation programme (EXCOSM, grant No. 101159513). KM is funded by Horizon Europe ERC grant no. 101125877. PW acknowledges support from the Science and Technology Facilities Council (STFC) grants ST/R000506/1 and ST/Z510269/1. R.D. gratefully acknowledges support by the ANID BASAL project FB210003. MN is supported by the European Research Council (ERC) under the European Union’s Horizon 2020 research and innovation programme (grant agreement No. 948381) and by UK Space Agency Grant No. ST/Y000692/1.

**DATA AVAILABILITY**

The set of SNID templates used throughout can be made available on request. Additionally, the full set of blended spectra used throughout are to be made available through a public repository on TBC.

**References**

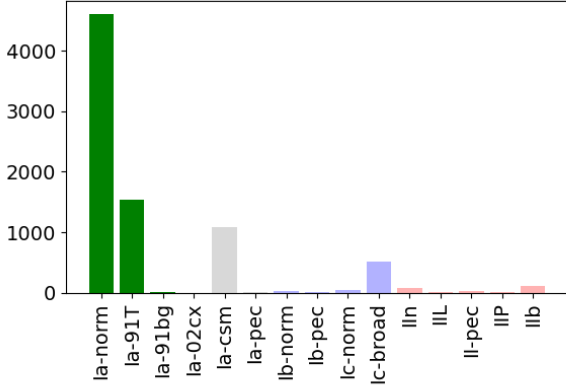
- Abbott T. M. C., et al., 2019, *ApJ*, 872, L30
- Astier P., et al., 2006, *A&A*, 447, 31
- Astropy Collaboration et al., 2013, *A&A*, 558, A33
- Balland C., et al., 2009, *A&A*, 507, 85
- Betoule M., et al., 2014, *A&A*, 568, A22
- Blondin S., Tonry J. L., 2007, *ApJ*, 666, 1024
- Blondin S., Tonry J. L., 2011, SNID: Supernova Identification, Astrophysics Source Code Library, record ascl:1107.001
- Brout D., et al., 2022, *ApJ*, 938, 110
- Campbell H., et al., 2013, *ApJ*, 763, 88
- Capaccioli M., ed. 1989, *The World of Galaxies*
- Cardelli J. A., Clayton G. C., Mathis J. S., 1989, *ApJ*, 345, 245
- Conley A., et al., 2011, *ApJS*, 192, 1
- DES Collaboration et al., 2024a, *arXiv e-prints*, p. [arXiv:2401.02929](https://arxiv.org/abs/2401.02929)
- DES Collaboration et al., 2024b, *ApJ*, 973, L14
- Dhawan S., et al., 2022, *MNRAS*, 510, 2228
- Drout M. R., et al., 2014, *ApJ*, 794, 23
- Duan F.-Q., Liu R., Guo P., Zhou M.-Q., Wu F.-C., 2009, *Research in Astronomy and Astrophysics*, 9, 341
- Dumayne J., et al., 2023, *RAS Techniques and Instruments*, 2, 453
- Filippenko A. V., 1997, *ARA&A*, 35, 309
- Fraga B. M. O., et al., 2024, *arXiv e-prints*, p. [arXiv:2404.08798](https://arxiv.org/abs/2404.08798)
- Gezari S., 2021, *ARA&A*, 59, 21
- Goldwasser S., Yaron O., Sass A., Irani I., Gal-Yam A., Howell D. A., 2022, *Transient Name Server AstroNote*, 191, 1
- Graham A. W., Driver S. P., 2005, *Publ. Astron. Soc. Australia*, 22, 118
- Guigliion G., et al., 2019, *The Messenger*, 175, 17
- Guy J., et al., 2007, *A&A*, 466, 11
- Guy J., et al., 2010, *A&A*, 523, A7
- Hakobyan A. A., Adibekyan V. Z., Aramyan L. S., Petrosian A. R., Gomes J. M., Mamon G. A., Kunth D., Turatto M., 2012, *A&A*, 544, A81
- Homeier N. L., 2005, *ApJ*, 620, 12
- Hounsell R., et al., 2018, *ApJ*, 867, 23
- Howell D. A., et al., 2005, *ApJ*, 634, 1190
- Hsiao E. Y., Conley A., Howell D. A., Sullivan M., Pritchett C. J., Carlberg R. G., Nugent P. E., Phillips M. M., 2007, *ApJ*, 663, 1187
- Ivezić Ž., et al., 2019, *ApJ*, 873, 111
- Jones D. O., et al., 2018, *ApJ*, 857, 51
- Jones D. O., et al., 2019, *ApJ*, 881, 19
- Kessler R., et al., 2009, *PASP*, 121, 1028
- Kessler R., et al., 2010, *PASP*, 122, 1415
- Kessler R., et al., 2019, *PASP*, 131, 094501
- Kim Y. L., et al., 2022, *PASP*, 134, 024505
- Kim Y.-L., et al., 2024, *arXiv e-prints*, p. [arXiv:2410.10963](https://arxiv.org/abs/2410.10963)
- Kinney A. L., Calzetti D., Bohlin R. C., McQuade K., Storchi-Bergmann T., Schmitt H. R., 1996, *ApJ*, 467, 38
- Leloudas G., et al., 2015, *MNRAS*, 449, 917
- Lidman C., et al., 2020, *MNRAS*, 496, 19
- Lochner M., McEwen J. D., Peiris H. V., Lahav O., Winter M. K., 2016, *ApJS*, 225, 31
- Mannucci F., Basile F., Poggianti B. M., Cimatti A., Daddi E., Pozzetti L., Vanzi L., 2001, *MNRAS*, 326, 745
- Minkowski R., 1979, *A Source book in astronomy and astrophysics, 1900-1975*. Harvard University Press
- Möller A., de Boissière T., 2020, *MNRAS*, 491, 4277
- Möller A., et al., 2022, *MNRAS*, 514, 5159
- Möller A., et al., 2024, *MNRAS*, 533, 2073
- Muthukrishna D., Parkinson D., Tucker B. E., 2019, *ApJ*, 885, 85
- Neill J. D., et al., 2011, *ApJ*, 727, 15
- Nugent P., Kim A., Perlmutter S., 2002, *PASP*, 114, 803
- Oke J. B., Gunn J. E., 1983, *ApJ*, 266, 713
- Perlmutter S., et al., 1999, *ApJ*, 517, 565
- Planck Collaboration et al., 2014, *A&A*, 571, A1
- Popper D. M., 1937, *PASP*, 49, 283
- Porter A. C., Filippenko A. V., 1987, *AJ*, 93, 1372
- Poznanski D., Gal-Yam A., Maoz D., Filippenko A. V., Leonard D. C., Matheson T., 2002, *PASP*, 114, 833
- Prugniel P., Simien F., 1997, *A&A*, 321, 111
- Riess A. G., et al., 1998, *AJ*, 116, 1009
- Rodney S. A., Tonry J. L., 2009, *ApJ*, 707, 1064
- Sako M., et al., 2011, *ApJ*, 738, 162
- Sako M., et al., 2018, *PASP*, 130, 064002
- Saunders W., et al., 2004, in Moorwood A. F. M., Iye M., eds, *Society of Photo-Optical Instrumentation Engineers (SPIE) Conference Series Vol. 5492, Ground-based Instrumentation for Astronomy*. pp 389–400, doi:10.1117/12.550871
- Savitzky A., Golay M. J. E., 1964, *Analytical Chemistry*, 36, 1627
- Schlegel E. M., 1990, *MNRAS*, 244, 269
- Scolnic D., et al., 2022, *ApJ*, 938, 113
- Sérsic J. L., 1963, *Boletín de la Asociación Argentina de Astronomía La Plata Argentina*, 6, 41
- Smartt S. J., et al., 2015, *A&A*, 579, A40
- Sullivan M., et al., 2006, *ApJ*, 648, 868
- Swann E., et al., 2019, *The Messenger*, 175, 58
- Tempel E., et al., 2020a, *MNRAS*, 497, 4626
- Tempel E., et al., 2020b, *A&A*, 635, A101
- Tyson J. A., 2002, in Tyson J. A., Wolff S., eds, *Society of Photo-Optical Instrumentation Engineers (SPIE) Conference Series Vol. 4836, Survey and Other Telescope Technologies and Discoveries*. pp 10–20 ([arXiv:astro-ph/0302102](https://arxiv.org/abs/astro-ph/0302102)), doi:10.1117/12.456772
- Vincenzi M., Sullivan M., Firth R. E., Gutiérrez C. P., Frohmaier C., Smith M., Angus C., Nichol R. C., 2019, *MNRAS*, 489, 5802
- Vincenzi M., et al., 2024, *arXiv e-prints*, p. [arXiv:2401.02945](https://arxiv.org/abs/2401.02945)
- Vogl C., Kerzendorf W. E., Sim S. A., Noebauer U. M., Lietzau S., Hillebrandt W., 2020, *A&A*, 633, A88
- Wittman D. M., Tyson J. A., Kirkman D., Dell’Antonio I., Bernstein G., 2000, *Nature*, 405, 143
- Yuan F., et al., 2015, *MNRAS*, 452, 3047
- de Jong R. S., et al., 2019, *The Messenger*, 175, 3

**APPENDIX A: SNE IA FITS AND CONTAMINANT ORIGINS**

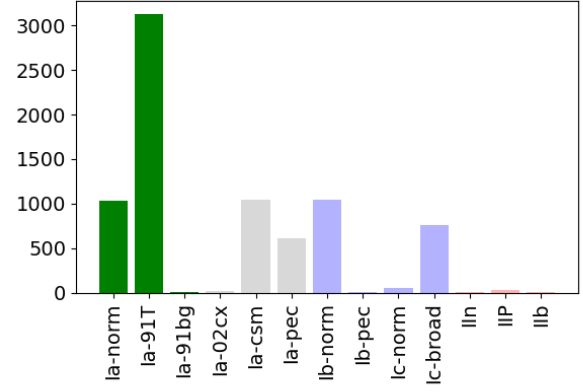
Fig. A1 shows how the SN Ia input spectra are being fit by each classifier. In each case the darker green bars indicate the good SN Ia classifications. The lighter green bars indicate SN Ia classifications below the quality threshold and non-SN Ia bars indicate all of the misclassifications. In all three classifiers we investigate we see the same effects of moving from using redshift priors to not.

There is a shift in successfully classified SNe Ia from the Ia-norm class into other SN Ia and SN Ia-pec subclasses. Additionally

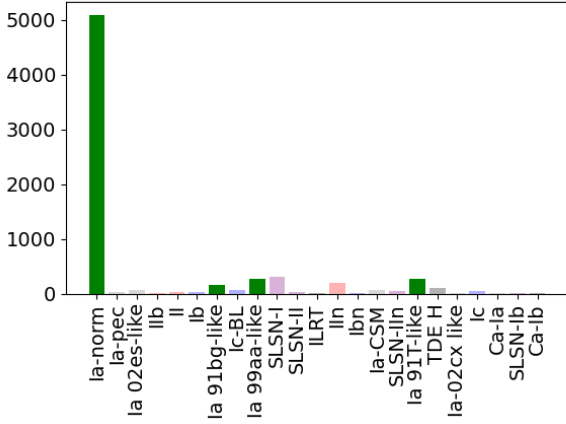




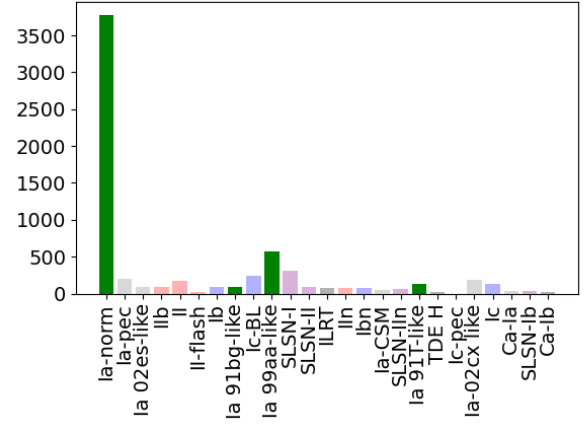
(a) DASH known z



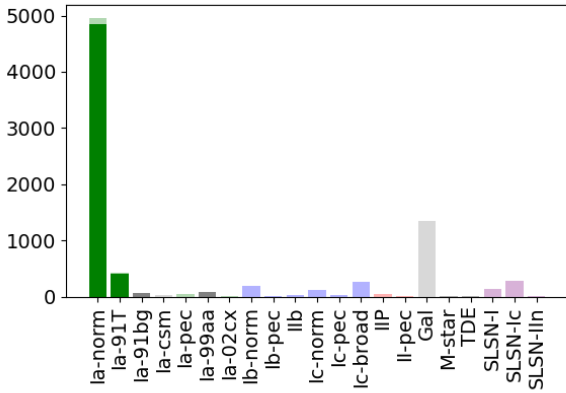
(b) DASH no z



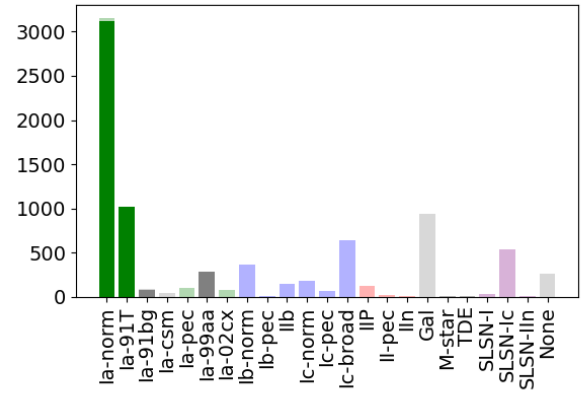
(c) NGSF known z



(d) NGSF no z



(e) SNID Known z



(f) SNID no z

**Figure A1.** Graphical representation of how SN Ia input spectra are being classified by each classifier with (left column) and without (right column) redshift priors. Each histogram lists only the subclasses with at least one classification. The lighter coloured green regions for SNID indicate the classifications that do not meet SNID’s *rlap* limit. SN Ia subclasses are green, Ibc are blue, II are red, SLSNe are purple, non-SNe are black and SN Ia-pec and non-transient classes are gray. The shift from Ia-norm to other SNe Ia subclasses when redshift priors are removed can be seen.

the number of SNe Ia incorrectly classified as non-SNe Ia can be seen in the non-green bars universally increasing in height. Both of these effects serve to diminish the SN Ia classification rate without redshifts.

SNID is the only classifier with a quality metric, and we see little change in the number of otherwise correct SN Ia classifications that fall below the quality cut. It appears that most SNe Ia classed as such are high quality classifications and most of the poor quality SN Ia classifications in the known redshift case are simply misclassified when the redshift information is removed.

Of note are the tendency of DASH to classify transients as SN Ia-csm. This seems to be the result of narrow galaxy emission lines from Sc host templates masquerading as the narrow lines of an ejecta-csm interaction. The inclusion of SN Ia-csm as an acceptable SN Ia class for DASH does improve the SN Ia classification rate, but at the cost of contamination rates exceeding 15%. A similar effect occurs with SNID, except that it does seem to prefer to correctly identify them as galaxies with a ‘Gal’ output.

Fig. A2 shows the origin of the contaminant results for each classifier. We can see immediately that DASH suffers as a result of having no ability to classify SLSNe, as they make up the largest fraction of contaminants when redshift priors are known.

When redshift information is removed, DASH loses classification performance for all transient classes, including contaminants. The fractional decrease in the number of SN Ia and contaminant classification is almost exactly the same, and this results in the FDR remaining low (see Tables 3 and 4). The input template classes that produce contaminants is entirely different when redshift priors are removed, now being almost entirely from SNe II. For SLSNe, forcing the classification to high redshifts by using priors resulted in many contaminant Ia classifications. When redshift priors are removed, SLSNe are instead misclassified as other non-SN Ia transients or as SNe Ia-pec. This is a good change from the point of view of SN Ia sample purity.

While we see the contaminant numbers produced by DASH maintained when removing redshift knowledge, NGSF and SNID both produce double or more contaminant SN Ia classifications. NGSF and DASH both classify predominantly SNe II as contaminant SNe Ia when redshift priors are removed, a significant change from the ratio of classes that produce contaminants with redshift priors. SNID’s distribution of contaminants remains almost identical between regimes, although again SNe II are the largest contributor.

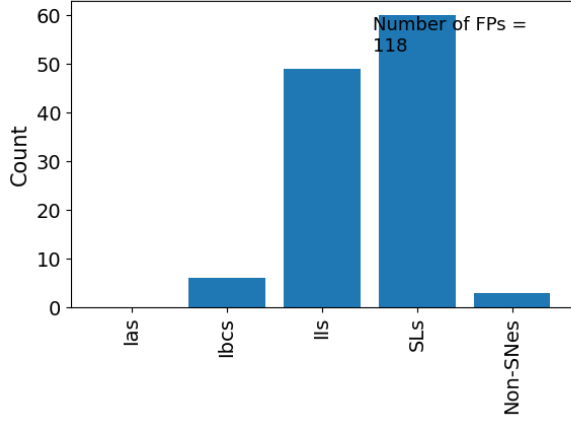
Type II SNe are the largest non-SN Ia component of the sample and as expected always dominate the contaminant distribution. In fact, in nearly all cases, the relative number of contaminants originating from the different input non-SN Ia classes at least vaguely mimics their relative abundance in the full sample, slightly shifted by each classifier’s ability to classify different classes. Only Fig. A2b bucks this trend, producing a large overabundance of SN II contaminant classifications.

## APPENDIX B: EXAMPLE CLASSIFICATION

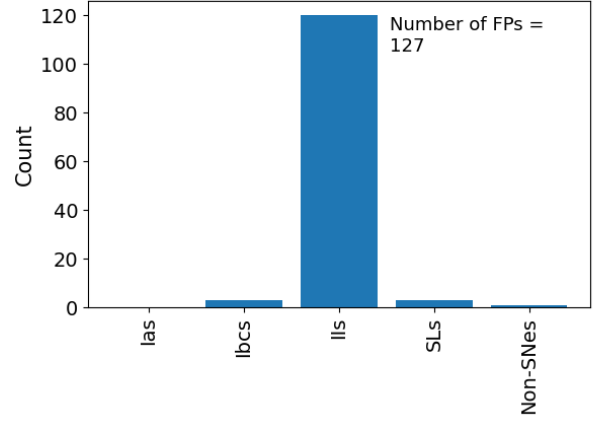
In this appendix we provide some individual classifications as context. We focus on several of the most common types of classification and misclassification. All presented classifications are from NGSF as it is the most prevalent in our suggested classification plan in Section 5.4.

Fig. B1 shows 4 attempted classifications with NGSF. Fig. B1(a) shows a successful SN Ia classification. We find that noisy spectra, where the transient is faint, or spectra with significant host contami-

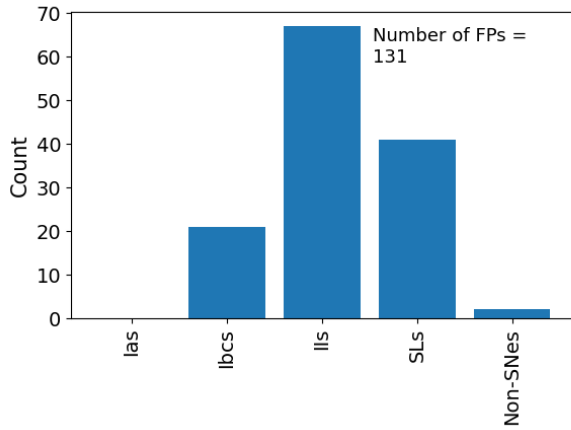
nation are often hard to classify as would be expected. This is shown in Fig. B1(b) We also see an overabundance of misclassifications from spectra with the Sc host template. These are often the result of the classifier misinterpreting the strong galaxy emission as narrow features from the transient. This leads to many classifications of SN Ia-csm (circum-stellar medium) and other narrow emission transient subclasses like Ibn, IIn etc. This is shown in Fig. B1(c). False positive SN Ia classifications can arise from many effects. Shown in Fig. B1(d) we have a low host contamination SN Ib being misinterpreted as a Ia-norm with significant host contamination. This suggests that there is degeneracy between SN subclass and host contamination levels.



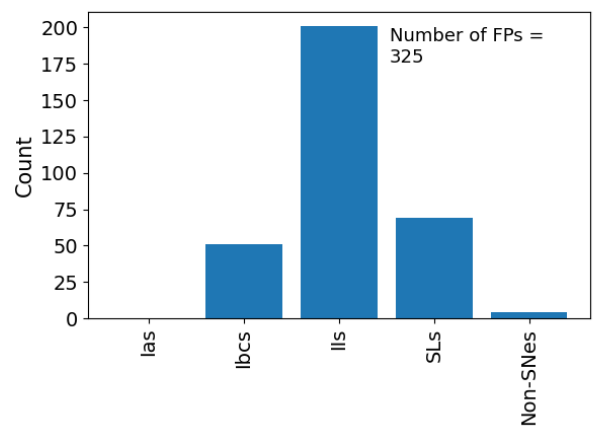
(a) DASH knownz



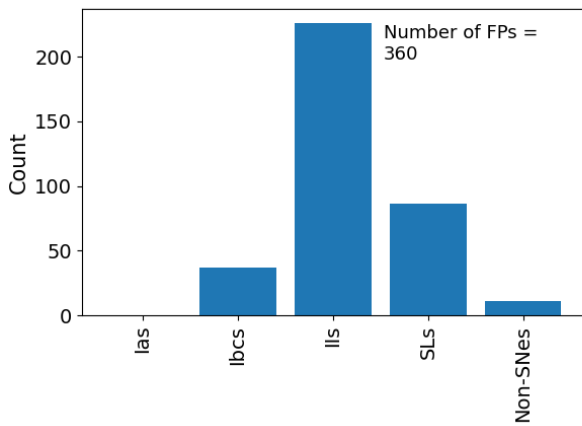
(b) DASH noz



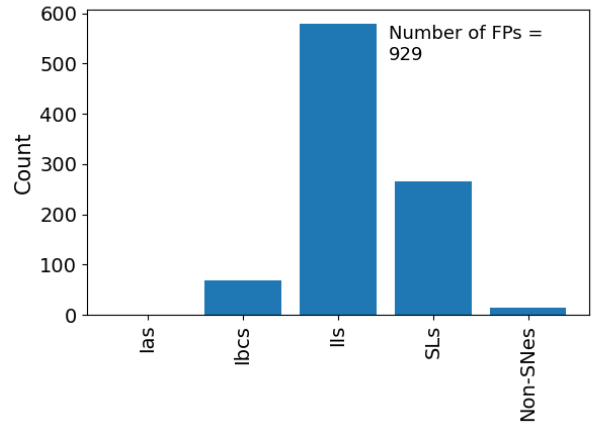
(c) NGSF knownz



(d) NGSF noz



(e) SNID Knownz



(f) SNID noz

**Figure A2.** The distribution of true classifications for objects classified as Ia above the quality threshold to qualify as contaminant results. Input classes are those from the 5-class classification schema. The number of contaminants for each classifier-redshift prior combination are listed on each subplot. The number of FPs increases significantly without redshift priors for NGSF and SNID. SLSNe are often over-represented as FP producers.

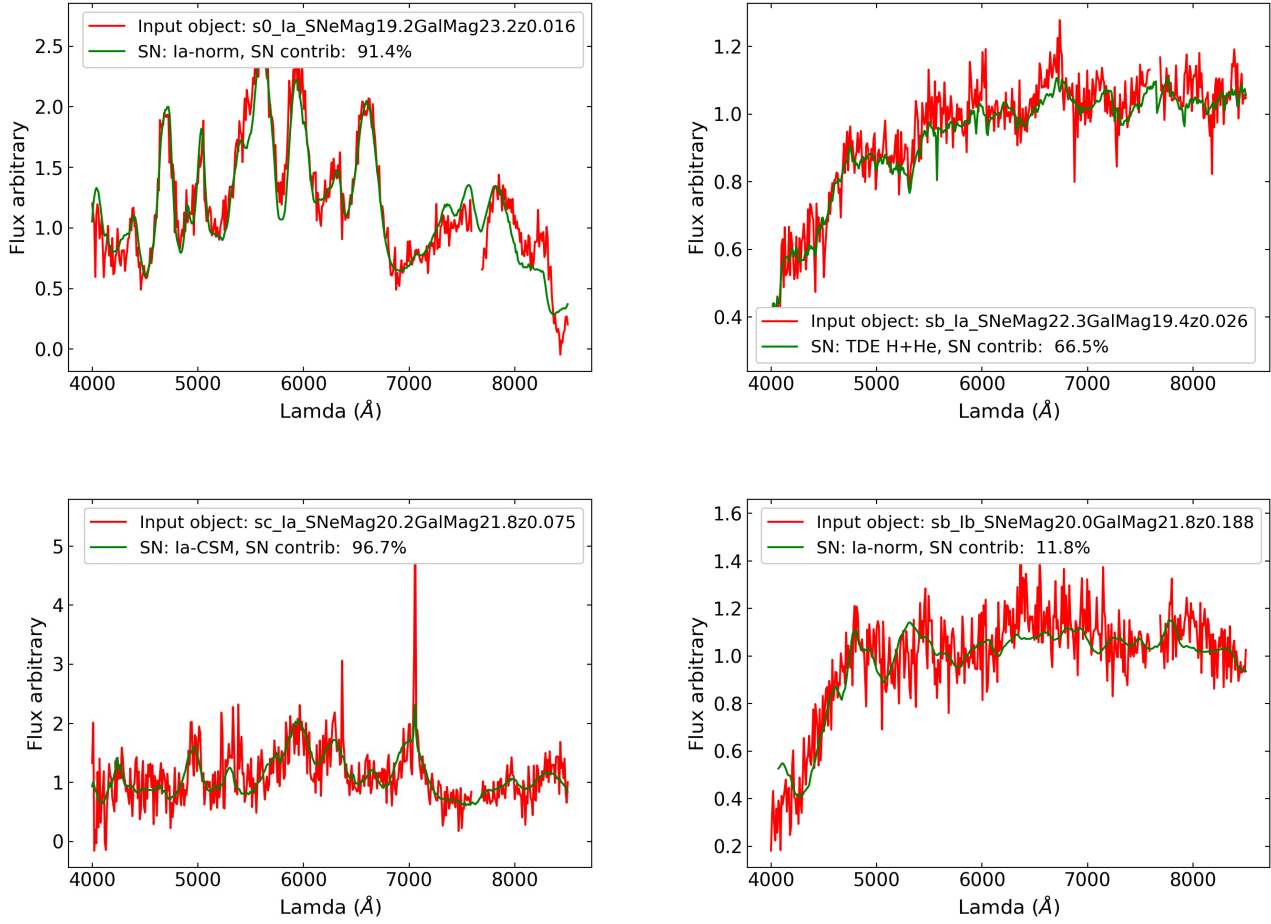


**Figure B1.** Four individual classification results from NGSF. (a) A good classification of a bright, low contamination SN Ia. (b) A misclassification of a highly contaminated SN Ia. (c) A misclassification of a bright SN Ia due to narrow galaxy features from its Sc host. (d) An example of a SN Ia false positive where a low contamination SN Ib is misinterpreted as a SN Ia with high contamination. In each case the input is plotted in red with relevant information in the legend. The best-fitting template spectrum is plotted in green and the best-fitting transient class is provided in the legend.